Institut für Wärmetechnik

TU Graz
Graz University of Technology

Raphael Gergely, B.Sc.

Simulation of a wood gasifier with combined heat and power

MASTERARBEIT

zur Erlangung des akademischen Grades

Diplom-Ingenieur

Masterstudium Maschinenbau
(Masterstudium Wirtschaftsingenieurwesen-Maschinenbau)

eingereicht an der

Technischen Universität Graz

Betreuer

Andres Anca-Couce, Priv.-Doz. Dipl.-Ing. Dr.-Ing.
Institut für Wärmetechnik

Beurteiler

Christoph Hochenauer, Univ.-Prof. Dipl.-Ing. Dr.techn.
Institut für Wärmetechnik

Graz, im März 2021

EIDESSTATTLICHE ERKLÄRUNG

AFFIDAVIT

Ich erkläre an Eides statt, dass ich die vorliegende Arbeit selbstständig verfasst, andere als die angegebenen Quellen/Hilfsmittel nicht benutzt, und die den benutzten Quellen wörtlich und inhaltlich entnommenen Stellen als solche kenntlich gemacht habe. Das in TUGRAZonline hochgeladene Textdokument ist mit der vorliegenden Masterarbeit identisch.

I declare that I have authored this thesis independently, that I have not used other than the declared sources/resources, and that I have explicitly indicated all material which has been quoted either literally or by content from the sources used. The text document uploaded to TUGRAZonline is identical to the present master's thesis.

_____ _____

Datum / Date Unterschrift / Signature

KURZFASSUNG

Titel: Simulation eines Holzvergasers mit kombinierter Nutzung von Wärme und Energie

Autor: Raphael Gergely

1. Stichwort: eindimensionales Strömungsmodell
2. Stichwort: Prozess Analyse
3. Stichwort: Gleichstrom Festbettvergaser

Ein effizienter Weg Holz zu nützen ist die Vergasung. Das Produkt dieses Prozesses ist das sogenannte Holzgas, welches in einer Vielzahl von Anwendungen seinen Einsatz findet. Eine Anwendung des Holzgases ist die Kraft-Wärme-Kopplung, in welcher das Holzgas zuerst über einen Wärmetauscher fließt und anschließend zum Betreiben eines Verbrennungsmotors verwendet wird.
Für diese Masterarbeit wurde die Simulation von Holzvergasern für die Kraft-Wärme-Kopplung bei kleinen Leistungen betrachtet. Diese Anwendung verlangt den Einsatz eines Gleichstromvergasers, da dieser Typ einen geringeren Teergehalt im Holzgas, verglichen mit anderen Vergasertypen aufweist. Die Kraft-Wärme-Kopplung für kleinere Leistungen verwendet meistens Kolbenmotoren, welche nur mit Holzgas mit minimalen Teergehalten betrieben werden können. Ein Nachteil der Gleichstromvergasung ist allerdings, dass sie eine sehr geringe Flexibilität in Bezug auf den Brennstoff aufweist (Feuchte und Partikelgröße). Außerdem ist dieser Prozess aufgrund der hohen Temperaturen, die in der Oxidationszone auftreten, schwer zu steuern.
Um den Prozess besser verstehen und ihn im Detail analysieren zu können, ist es das Ziel dieser Masterarbeit die Gegenstromvergasung für einen Kraft-Wärme-Kopplung zu simulieren. Für diese Simulation wurde ein 1-dimensionales Strömungs-Modell verwendet.
Die Basis für das Modell bildete eine Simulation für Gegenstromvergasung, welche bereits validiert wurde. Dieses Modell wurde den Bedürfnissen einer Gleichstromvergasung angepasst. Aufgrund der komplexen Aufgabenstellung wurde das System zuerst in Untersysteme zerlegt. Eine Literaturrecherche ergab eine Vielzahl verschiedener Reaktionkinetiken, welche für ähnliche Modelle verwendet wurden. Diese Reaktionsraten wurden untersucht und mit experimentellen Daten validiert. Folgende Subprozesse wurden betrachtet: Aufheizung und Trocknung, Pyrolyse, Oxidation und Vergasung.
Der erste Subprozess, der validiert wurde, ist die Vergasung der Holzkohle. Dieser Prozess ist wichtig für die Stabilität und die Effizient des gesamten Systems. Um den Prozess zu validieren, wurde auf experimentelle Daten aus der Literatur zurückgegriffen. Zuerst wurden die Reaktionskinetiken für die Holzkohlevergasung betrachtet. Für eine bessere Darstellung der Ergebnisse aus dem Experiment wurden Wassergas-Shift-Reaktionen zur Simulation hinzugefügt.
Die nächsten Subprozesse, welche betrachtet wurden, sind die oxidation-Zone und die Pyrolyse. Die oxidations-Zone ist schwierig zu kontrollieren und kann zu instabilen Prozessen führen. Die ersten Simulationen, die mit inerter Pyrolyse Modell durchgeführt wurden, führten zu keinen zufriedenstellenden Ergebnissen. Daraufhin wurde die inerte Pyrolyse durch eine oxidative Pyrolyse ersetzt, welche aufgrund ihrer exothermen Natur dazu beigetragen hat, den Prozess autothermal ablaufen zu lassen und diesen damit zu stabilisieren.
Für die oxidations-Zone wurden wieder verschiedene Reaktionskinetiken aus der Literatur getestet, welche dann wieder mit experimentellen Daten validiert wurden. Das Cracken der primären Teere wurde auch in diesem Schritt in die Simulation eingeführt
Nachdem die Subprozesse validiert worden sind, wurde der Prozess als Ganzes simuliert. Die Reaktionsraten und chemischen Reaktionen wurden hierfür mit dem Wissen der vorherigen Simulationen ausgewählt. Für die Validierung der Ergebnisse wurde Daten des Vergasers, welcher sich am Institut befindet verwendet.
Das Modell ist nun validiert und kann für zukünftige Simulationen verwendet werden, wobei es dazu genutzt werden kann die Temperaturen im Reaktor vorherzusagen und die Zusammensetzung des Holzgases zu bestimmen.

ABSTRACT

Title: Simulation of a wood gasifier with combined heat and power

Author: Raphael Gergely

1st keyword: one-dimensional flow model
2nd keyword: process analysis
3rd keyword: fixed-bed downdraft gasification

An efficient way to energetically utilize wood, is gasification. The product of this process is the so-called producer gas, which can be employed in a variety of ways. One way of using the producer gas is in a combined heat and power cycle (CHP), where the producer gas first flows through a heat exchanger before being combusted in an internal combustion engine.

For this master thesis, small scale CHP gasification was investigated. Downdraft gasification is being used for this type of application due to its lower tar content in comparison to other gasification types. Small scale CHP gasification typically use internal combustion piston engines, which need a producer gas with minimal tar content.
The downside of the downdraft gasifier is its low flexibility when it comes to fuel intake (moisture and size of biomass particles). Moreover, due to the oxidation zone, where particularly high temperatures occur, the process is difficult to control.

To better understand the process and for a more detailed analysis, the goal of this master thesis was to simulate downdraft gasification for CHP processes. The simulation model which was used is a one-dimensional flow model.

To build the simulation an existing model for updraft gasification was used, which was already validated and then modified according to the needs of downdraft gasification. Because of the complexity of this task, the model was first divided into sub-processes. In literature, several reaction kinetics for the chemical reactions were found. These kinetics were investigated and validated with experimental data. The gasification process consists of the following sub-processes: heating and drying, pyrolysis, oxidation, and gasification.

The first sub process which was investigated was the gasification of charcoal. The gasification zone is essential for the process´ stability and efficiency. For the validation of the gasification zone experimental data from literature was used. The reactions validated in this step were the gasification of the charcoal with H_2O and CO_2. To further increase the accuracy of the simulation the water gas shift reactions were added.
The next sub-processes that were validated, were the pyrolysis and the oxidation zone. The oxidation zone is difficult to control and can lead to an unstable process. Because of the unstable nature of the first simulations, conducted with inert pyrolysis, an oxidative pyrolysis scheme was developed. This new pyrolysis scheme helped to stabilize the process due to its exothermic nature, which helped to keep the process autothermal.
The gas phase oxidation was also validated in the same sub process. Several different reaction kinetics from literature were used in simulations and then compared to the experimental results. Tar cracking reactions were also added as well in this step.
After the sub processes were validated, the whole process was simulated. For the simulation, reaction kinetics from previously validated sub-processes were used. Also, secondary tar cracking reactions were added at this step, to better predict the tar content. The results of this simulation were then compared to experimental data from the downdraft gasifier which is located at the institute and provided by an industrial partner.
The model is now verified and can be used for further simulations. The main uses for the model are to predict the temperatures in the reactor and the composition of the producer gas.

PREFACE

This master thesis was written in 2021 at the IWT institute, it should help to analyse the process of downdraft gasification.

I want to thank Priv.-Doz. Dipl.-Ing. Dr.-Ing. Andres Anca-Couce and Univ.-Prof. Dipl.-Ing. Dr.techn. Christoph Hochenauer for their supervision of the master thesis.

I want to acknowledge the “Advanced-Bio-CHP” project, by the Austrian Research Promotion (FFG), which made this master thesis possible.

I also want to thank M. Buchmayr and J. Gruber from Hargassner GesmbH for their cooperation with TU Graz and A. Zachl.

I also want to thank my parents for supporting me through my whole education.

Graz, 26.03.2021

Raphael Gergely

TABLE OF CONTENTS

Nomenclature	
A	pre-exponential factor (1/s) area (m^2)
c_p	specific heat capacity (J/ (kg))
D	mass dispersion/ diffusivity (m^2/s)
d_p	particle diameter (m)
E	activation energy (J/mol)
F	friction terms in momentum equation ($kg/(m^{2\,2})$)
f_1	first friction factor ($kg/(m^3\ s)$)
f_2	second friction factor ($kg/(m^4)$)
f_{Shr}	shrinkage factor (–)
$f_{Shr\text{-}min}$	minimum shrinkage factor (–)
G	conductance (W/K)
H	convective and viscous terms in the momentum equation ($kg/(m^2\ s^2)$)
$\dot{H}$	advection rate (W)
M_m	molecular weight (kg/mol)
Nu	Nusselt number (–)
p	pressure (Pa)
Pr	Prandtl number (–)
$\dot{Q}$	heat transfer rate (W)
r	radial coordinate of particle (m)
$\dot{r}$	reaction rate per unit volume ($kg/(m^3\ s)$)
R	universal gas constant (J/(mol K))
R_c	source term in continuity equation ($kg/(m^3\ s)$)
Re	Reynolds number (J/(mol K))
s	ration surface/volume of the particle (1/m)
T	temperature (K)
t	time (s)
V	Volume (m^3)
v	general vectorial velocity (m/s)
v	particle superficial velocity (m/s)
w_z	reactor axial velocity (m/s)
Y	mass fraction (–)
z	axial coordinate of the reactor (m)
α	heat transfer coefficient ($W/(m^2\ K)$)
β	mass transfer coefficient (m/s)
Δh	heat of reaction (J/kg)
ϵ_r	porosity (–)
η	conversion factor (–)
κ	permeability (m^2)
λ, Λ	thermal dispersion/ conductivity (W/(m K))
μ	viscosity (kg/(m s))
ν	stoichiometric coefficient (–)
ρ	density (kg/m^3)
ζ	Stefan correction (kg/m^3)

Table 1: Nomenclature

Subscripts	
0	initial value
b	relative to the fixed-bed
c	relative to char
e	relative to the energy equation
down	downstream
eff	effective
g	pertains to gas phase
i	pertains to specie with index i
j	pertains to reaction with index j
p	relative to the particle
up	upstream
VC	control volume
w	relative to wood

Table 2: Nomenclature subscripts

1 INTRODUCTION

To reduce the global emissions of greenhouse gases and contain global warming, alternatives for fossil fuels must be used. Biomass, a renewable energy source with global availability, is one such alternative.
An efficient way to utilize biomass is its gasification. To further increase its efficiency, gasification can be used in a combined heat and power cycle (CHP). This technology can provide electricity at a higher efficiency, as on processes that are based on combustion. In the CHP cycle, wood is being converted into producer gas through gasification before its combusted in an internal combustion engine. Heat can be obtained either from losses of the engine, the flue gas and from the cooling of the producer gas before it enters the engine. This configuration is typical for small- and medium-scales but can reach up to a thermal output of 26 MW_{th}[36].

For this master thesis, gasification with a CHP cycle for small-scales was investigated. A small-scale gasifier can be used to provide a reliable and independent source of heat as well as electricity for rural areas [25]. The internal combustion engines, which are used for the small scales, require producer gas with a low tar content. The requirement of gas cleaning is a hinderance for the development of small-scale CHP gasification. Therefore, downdraft gasification is used for this application as this technology provides producer gas with lower tar content compared to other technologies.
A commercially available downdraft gasifier (85 kW), which was developed for small-scale CHP cycles, is used for research at the IWT institute of the TU Graz. Data from this research activities was used in this master thesis to validate the simulations.
A downside of this reactor is its low flexibility in terms of fuel variety, which is limited regarding its particle size or fuel moisture content. The process is also a challenging one concerning its control because of the high temperatures that occur in the oxidation zone. Even though downdraft gasifiers produce less tars than other technologies, the tar content is still critical and should be minimized.

To improve the aspects mentioned before, a thorough understanding of the problem is required. Therefore, the aim of this master thesis is to simulate the process of downdraft gasification by using a one-dimensional flow model to analyse the process in detail and gain a better understanding of it. The knowledge gained from the simulations can be used to develop future control strategies.

The starting point for the downdraft gasification model was a previously validated model for updraft gasification by Anca-Couce et al. [38]. This model was adjusted according to the needs of downdraft gasification. To adjust the model, suitable parameters and reaction kinetics had to be found in literature. The model was then divided into sub-processes for an easier validation of the simulation parameters and the reaction kinetics. For this validation suiting data was taken from experiments, provided in literature.
After the sub-processes were validated, the whole process was validated; all sub-processes are active during this step. This was done with the experimental data taken from the gasification reactor located at the institute.

2 THEORETICAL FOUNDATIONS

2.1 Bioenergy

2.1.1 Biomass

Biomass is made up of carbon-based organic matter.

Types of biomass are:

- Plants and animals
- Resulting residues of plants and animals
- Dead (but not fossil) Plants and animals, (e.g. straw)
- Substances that resulted from biomass (e.g. paper)

[1]

2.1.2 Utilization of biomass

Biomass can be utilized for heating, production of electricity and transportation (fuel).
[9]

For heating, the biomass is usually combusted in boilers, furnaces or stoves. In developing countries biomass is mostly simply burnt for cooking and heating, which leads to high emissions and low efficiencies. Therefore, this method is not renewable. The most widely used forms of biomass for heating are wood logs, chips or pellets. Due to innovative technologies in biomass combustion, such as air staging, emissions were reduced, while the overall efficiency was increased. [2]

In transportation, two main type of fuels are being used: biodiesel and bioethanol. In Austria, for instance, biodiesel and ethanol are blended with regular fuels by law (7% biodiesel in B7, 5% ethanol in E5 gasoline). Biodiesel is made from vegetable oils and bioethanol from starchy crops via fermentation. [26]

There exist three generations of biofuels. First generation biofuels are made from crops and are slightly better than traditional fuels in terms of their overall carbon footprint. They also compete with food productions when it comes to cultivable land.
Second generation biofuels are made of lignocellulosic biomass or waste. It is more difficult to extract the fuel from them, yet they have a lower carbon footprint and no conflicting competition with food manufacturing.
Third generation biofuels are made of algae. Currently, this process is not commercially available.
[2]

To produce electricity from biomass, several technologies can be applied:
.

- Combustion of solid biomass derived from wood or agricultural biomass combined with Rankine cycle
- Combustion of biogeneous fraction of municipal solid waste combined with Rankine cycle
- Biogas from digestion combined with gas engine
- Gasification of biomass combined with gas engine

To increase the efficiency of the electricity production, a combined heat and power cycle (CHP) is being used. During this process, the waste heat of the process is used for heating. Several options are available for CHP depending on the fuel and the power output.

For combustion and gasification, which is the focus of this master thesis, a combined heat and power cycle (CHP) is used to produce electricity. For combustion two options are used: a steam cycle for medium and large scale (2 MW_{el} – 1000 MW_{el} [27]) and an organic Rankine cycle for small scale processes (100kW_{el} – 2MW_{el} [27]). The electric efficiency for biomass combustion in CHP is around 20% [2](plants with several MW_{el}).

For CHP with gaseous or liquid fuel, the most common option is to use an internal combustion engine. The fuels which can be used are biogas from digestion, landfill gas or gas from gasification. Another method is to burn the fuel in a turbine, which is used for larger scales.

One method of using CHP for gas engines with solid fuel is gasification. During this process, the solid biomass is converted to producer gas, which is then burnt in an internal combustion engine. The electric efficiency that results from this process is higher (30%) compared to combustion (20%). Before entering the engine, the gas has to be cooled to increase its density. The heat generated from the cooling process can be used for the CHP. The exhaust heat is used for the CHP cycle too, as well as the thermal losses of the engine. The tar content and the particle mater of the producer gas must be below 50 mg/Nm^3 for tars and below 50 mg/Nm^3 for PM [20]. To achieve such low tar content, gas cleaning is required. This, however, has hindered the development for CHP with gasification.[21]
For small scale CHP gasification, fixed-bed downdraft gasification is being used. These systems require less gas cleaning due to their lower tar output. The downside of these reactors is the low flexibility of the fuel (low moisture content and strict specification for size are required). This master thesis focusses on simulating these reactors to analyse and, consequently, better understand the process.
Another way of using the producer gas would be to combust it in a turbine. The efficiency of turbines is similar to that of gas engines. Here, tar cleaning is not necessary. The turbines require gas with a high caloric value, which is challenging for biomass gasification.
[2]

2.1.3 Biomass conversion

To receive energy from biomass, it is possible to either directly combust the biomass, or to obtain it through the conversion to a secondary energy source, which can be used in a second process (e.g. syngas from gasification).
There are three ways for the conversion:

- Physico-chemical conversion, which is used to provide biofuels from vegetable oils.

- Bio-chemical conversion, which uses the fermentation of sugar or starch to produce ethanol. Another method is to use anaerobic digestion, which produces biogas.

- Thermo-chemical conversion, which consists of: combustion, gasification, pyrolysis, hydrothermal liquefication and hydrothermal carbonization. The products of these processes:

  - Combustion: Heat, CO_2, H_2O, ashes
  - Gasification: CO, H_2, CH_4, CO_2, H_2O, ashes
  - Pyrolysis: Bio-oil, biochar, gases
  - Hydrothermal carbonization: Hydro-char

[1]

2.1.4 Thermo chemical conversion

The aim of thermo-chemical conversion is to chemically alter solid biomass under the influence of heat to provide thermal energy and/or refined solid, liquid, and gaseous fuels. [9]

The four main processes of thermo-chemical conversion are the following: heating and drying, pyrolysis, gasification, and oxidation/combustion. [9]

Heating and Drying

Temperatures up to 200°C cause water to evaporate due to the porous structure of the biomass. That is an endotherm process and, therefore, requires energy. The temperature stays approximately the same until the biomass has fully dried. [1]

Pyrolysis

Pyrolysis takes place at temperatures between 250 and 400°C under inert atmosphere. Macromolecules from the biomass are divided into the following reaction products:

- Char
- Pyrolytic liquids (tars and water)
- Permanent gases: CO, CO2, CH_4 and H_2 and C_xH_y

[1]

Gasification

Gasification takes place under a reducing atmosphere, at temperatures higher than 600°C. It is a sub-step to complete oxidation, but can also be used to produce syngas, which can be combusted later. The products of pyrolysis react in the gasification phase with a gasification agent (CO_2 or H_2O or O_2 under a lambda of 0.2 – 0.3). An essential part of gasification is the conversion of the left-over solid carbon components of the pyrolysis to combustible gases.
[1]

Oxidation/Combustion

Oxidation, which is highly exothermic, takes place at a lambda > 1 and at temperatures above 1000°C. Solid carbon components and combustible gases can be oxidized [1].

2.2 Gasification process

There are two main types of gasification: autothermal, where the heat source is provided by partial oxidation in the gasifier and allothermal where the heat source is external.

The most common medium for gasification is air, yet due to the high nitrogen amount in air, the producer gas is diluted and, therefore, has a lower heating value. Gasification with oxygen or steam increase the heating value of the producer gas.

The reactions which take place when biomass is gasified are the following:

First wet biomass is dried and the water in it is evaporated in form of steam, then pyrolysis takes place, where the dry biomass is converted to char, condensable species (tars, H_2O) and permanent gases (CO, CO_2, C_xH_y). The char is then oxidized with the introduction of the oxidation medium. After the oxidization, the gasification of the char takes place. The product gas from the gasification can contain CO, H_2, CH_4, CO_2. N_2, Ash. Unconverted char and tars are the by-products of the reaction. The main reactions in gasification are shown in Figure 1 and in the equations 1 - 11.
[1]

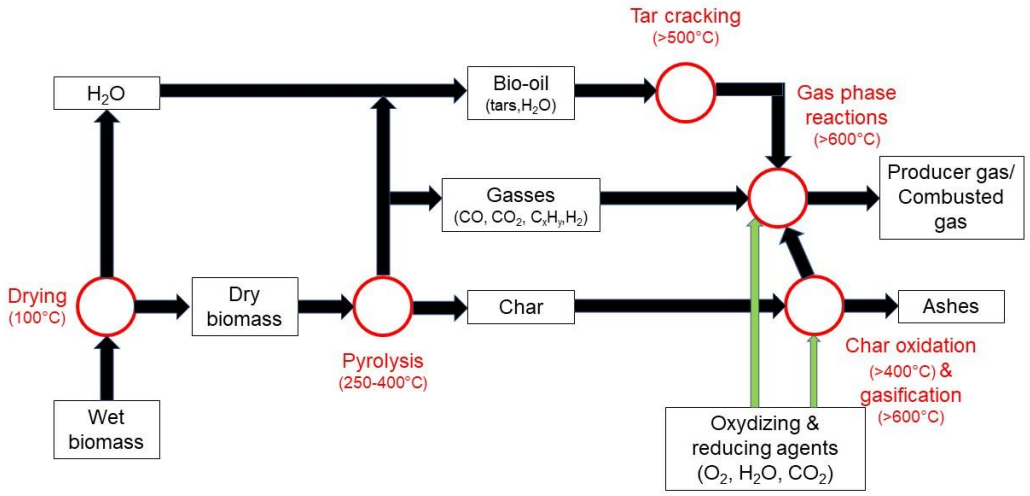

Figure 1: Summary of reactions during gasification

Equation 1 shows the general chemical reaction of gasification with air. More detailed reactions are depicted in the next equations, which are separated into the sub-processes.

$$C_x H_y O_Z + O_2 + (N_2) \rightarrow CO + H_2 + CO_2 + H_2O + Tars + CH_4 + (N_2)$$

Equation 1: Gasification reaction λ=0.2-0.3

In the drying zone the following reactions take place:

$$\text{Wet biomass} \rightarrow \text{Dry biomass} + H_2O_{(g)}$$

Equation 2: Chemical reaction drying

The following reactions describe the pyrolysis zone. The exact yields that were used for the simulation are shown later in Table 15.

$$\text{Dry biomass} \rightarrow \text{Char} + \text{permanent gases} + \text{condensable species}$$

Equation 3: Chemical reaction pyrolysis

$$\text{Tar} \rightarrow 0.325\ CO + 0.325\ CO_2 + 0.1\ H_2O + 0.25\ \text{secondary tar}$$

Equation 4: Chemical reaction prim. tar cracking

The chemical reactions for the oxidation zone are the following:

$$CHxO_y + (1 - \eta/2 + x/4 - y/2)\ O_2 \rightarrow \eta\ CO + (1 - \eta)\ CO_2 + x/2 H_2O$$
$$\eta = f(T)$$

Equation 5: Chemical reaction char oxidation

$$CO + 0.5\ O_2 \rightarrow CO_2$$

Equation 6: Chemical reaction CO oxidation

$$CH_4 + 1.5\ O_2 \rightarrow CO + 2H_2O$$

Equation 7: Chemical reaction CH_4 oxidation

$$H_2 + 0.5\ O_2 \rightarrow H_2O$$

Equation 8: Chemical reaction H_2 oxidation

The gasification zone is described by the following reactions:

$$CH_xO_y + (1 - y)\ H_2O \rightarrow CO + (1 + x/2 - y)\ H_2$$

Equation 9: Chemical reaction char gasification with H_2O

$$CH_xO_y + CO_2 \rightarrow 2\ CO + (x/2 - y)\ H_2 + y\ H_2O$$

Equation 10: Chemical reaction char gasification with CO_2

$$CO + H_2O \rightarrow CO_2 + H_2$$

Equation 11: Water gas shift

2.3 Applications of producer gas

The producer gas can be utilized in the following ways:

- Heat and power
- Production of liquid and gaseous fuel
- Synthetization of chemical and organic compounds.[1]

2.3.1 Power production from producer gas

Power production can be achieved through with an CHP cycle, which was described in chapter 2.1.2. Other methods include realising a conventional steam cycle, heated by combusting the producer gas or fuel cells. The steam process is not done in reality because it would have a lower efficiency than simply combusting the biomass.
When the producer gas is used in fuel cells it needs extensive cleaning especially of sulphur. Moreover, the technological development of fuel cells is lower than for other technologies.
[2]

2.3.2 Production of liquid fuels

Both, liquid and gas fuels can be made from producer gas. A diesel-like fuel can be produced by the so-called Fischer-Tropsch synthesis. A gasoline-like fuel can be made from methanol, which can be won from the producer gas. It is necessary to clean the producer gas before the synthesis to avoid catalyst poisoning.
H_2 and CH_4 can be made from producer gas. Firstly, the gas is cleaned of tars, sulphur and other unwanted products. Then, gas shift reactions are used to obtain the desired products. In the final step, the desired gases are separated through condensation, adsorption, or a membrane, for instance.
[1]

2.4 Gasification reactors

The three main types of reactors are fixed bed reactors, fluidized bed reactors and entrained flow reactors. Those can be further categorized into sub-types.

Table 3 shows the typical thermal power range and the tar output for the technologies. The main difference between these three reactor types is that in the fixed bed gasifier the fuel particles are not moved by the velocity of the incoming gas stream. In fluidized reactors, the velocity of the gas stream is high enough to move the solid particles. In entrained flow, the fuel is injected in particle form with the gasification medium. [1]

Gasification technologies		
	Power range [MWth]	Tars [g/Nm^3]
Fixed-bed downdraft	0.1 - 2	< 1
Fixed-bed updraft	1 - 5	< 100
Fluidized bed	5 - 50	< 10
Entrained flow	> 50	< 0.1

Table 3: Gasification technologies

2.4.1 Fluidized bed reactors

The velocity of the incoming gas is high enough for the solid fuel particles to start moving. The bed consists of an inert material, such as quartz sand, which is evenly mixed with the fuel. There are no distinct zones for the gasification process. The sub-processes take place parallelly. [1]

Bubbling fluidized bed

Bed material stays in the reactor, due to the lower velocities of incoming gas. Material is evenly distributed throughout the reactor. [1]

Circulating fluidized bed

Bed material escapes the reactor due to high velocities. Cyclones are used to separate the bed material from the gas and recirculate it back to the reactor. [1]

2.4.2 Entrained flow

The fuel is injected with the gasification medium (oxygen and steam are most common) at temperatures above 1200°C. Because of the small particle size and the high temperatures, the fuel is being gasified in in merely a couple seconds. This reactor type is rarely used for biomass gasification. [1]

2.4.3 Fixed bed reactors

In a fixed bed gasifier, the solid fuel is put in at the top of the reactor in a bulk. Because of the discharge of residue in the bottom of the reactor, the solid fuel moves slowly through the reactor, due to gravity. The gasification medium is put in, at the top or in the oxidation zone for downdraft gasifiers and at the bottom for updraft gasifiers. The fuel is then passing the different zones of the reactor. Drying, pyrolysis, char gasification and oxidation are taken place in separated layers, which are clearly distinguished. [1]

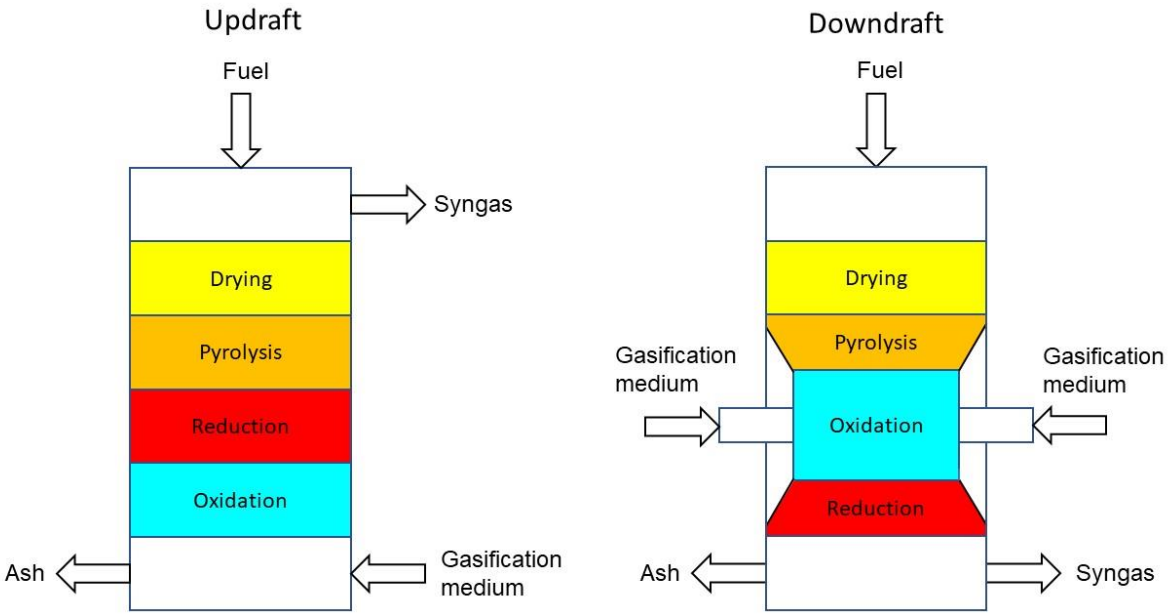

Figure 2: Updraft Downdraft fixed bed

Updraft gasification

Solid fuel is being added at the top and travels downwards. The gasification medium enters at the bottom and travels upwards. There is a clear distinction between the zones, where the sub-processes take place. The gasification medium, first travelling through the oxidation zone and transports a part of the thermal energy to the layers above. The next layer is the reduction zone where oxidation products (CO_2, H_2O) are partly reduced to CO and H_2. Then, the gas is passed through the cooler zones of the reactor. The next one is the pyrolysis zone, where the thermochemical splitting of the biofuel takes place under the influence of the heat from the gas. The last zone the gas passes is the drying and heating zone. Afterward, the gas escapes the reactor at a relatively low temperature of around 100-200°C. Updraft gasification is used for thermal power outputs from 1MW to 5MW.

Advantages:

- Simple Process
- Fuel flexibility (moisture, particle size)
- High efficiency
- Low dust content
- Low temperature of produced gas

Disadvantages:

- High tar content
- Danger of channelling and bridging

[1]

Downdraft Gasification

Solid fuel is added at the top of the reactor and travels downward. The gasification medium is either added at the top or at the oxidation zone, as shown in Figure 2. At the top of the reactor there is the drying and heating zone. In this zone, the solid fuel is heated, and water evaporates in the form of steam (Equation 2). One layer below the pyrolysis zone can be found, where solid fuel is thermochemically split into pyrolysis gases and char (Equation 3) and primary tars are cracked (Equation 4). These zones take place in a relatively oxygen-free atmosphere. The produced gases then pass the oxidation zone. There, the char that was produced during the pyrolysis phase reacts with oxygen (Equation 5). As this is a highly exothermic reaction, the temperature rises above 1000°C. The combustible gases from the pyrolysis (CO, CH_4, H_2) partly react with oxygen as well and H_2O and CO_2 result as products (Equation 6, Equation 7, and Equation 8). In the succeeding reduction zone, H_2O and CO_2 react with char at bottom of the reactor bed and are reduced to CO and H_2 (Equation 9 and Equation 10). The produced gas is escaping the reactor at temperatures of around 600 to 800°C.

Advantages:

- Simple process
- Lower tar content

Disadvantages:

- Limits in feed size, moisture and maximum ash content
- Limited scale up
- Danger of bridging and clinkering
- Difficult to control the oxidation zone, due to its high temperature

[1]

2.5 Motivation for simulation

For this master thesis, a small-scale gasifier, which is used for a CHP cycle, had to be simulated. Downdraft gasification is ideal for this process, because it is suited for smaller scales and has a lower tar content compared to other gasifier types (Table 3).

The tar content is still highly critical for running a CHP cycle with an internal combustion piston engine and, therefore, needs to be minimized as much as possible. The requirement of gas cleaning hinders the development of small sale CHP gasification. The process of the downdraft gasification is also difficult to control, due to the oxidation front where high temperatures are needed. The downdraft gasification for a CHP has a low flexibility for fuel intake (low moisture content and strict specifications for particle size). A better understanding of the whole process is required to improve this aspect.

Due to the process limitations, the simulation in this master thesis aims to analyse the process in more detail for a better understanding. Furthermore, this knowledge can be used to develop control strategies for this process.

3 MODEL DESCRIPTION

The model that was used for the simulations, is based on a one-dimensional flow model for updraft gasification[38].
Solid fuel as well as the gasification agent are added at the top of the reactor. The producer gas and unconverted mass escapes at the bottom of the reactor.

The main reactions taking place during each sub-process are the following (the reactions are shown in Figure 1, the zones of the reactor are shown in Figure 2):

- Drying
- Pyrolysis: pyrolysis, tar cracking
- Oxidation: Char oxidation; CO, H_2, CH_4 oxidation
- Reduction: Char gasification with CO_2 and H_2, water gas shift

A shrinking core model is used to describe the char conversion. Other reactions are volumetric reactions. The gas velocity can be calculated with the Darcy law (Equation 16). Here, pressure, density, and temperature are coupled with the ideal gas law (Equation 17).

For the boundary conditions the following parameters are required:

- Biomass mass flow, composition and temperature
- Moisture content of biomass
- Inlet gas mass flow, composition and temperature
- Thermal resistance of insolation
- Outside temperature
- Heat loss bottom
- Heat input from top

Mass transfer, energy transfer and chemical reaction are discretised and solved along the reactor

3.1 General assumptions of the model

For all the simulations which were done for this master thesis, the following assumptions for the code were taken:

- Cylindrical reactor with constant porosity
- Quasi continuous model for gas and solid phase
- Spherical biomass particles, which are thermally thin, no intra-particle temperature
- In the drying/pyrolysis zone the solid bulk density is reduced. Particle size and solid velocity are assumed to be constant in the drying zone.
- Shrinking core model. The bulk density of the bed stays constant. The particle size and velocity are reduced during the conversion. When the volume is reduced the solid velocity is reduced proportionally to keep the bulk density constant.
- Gas phase components are ideal gases.

3.2 Mass and energy balances

In the model, there are two phases present, the solid phase, which also contains the liquid phase and the gas phase. For both species, the energy and the mass transport equations are solved along the reactor (Equation 4 – 7). To calculate the temperatures directly through the energy equations, these equations are given in a non-conservative form and are valid for low Mach numbers. [13]

For the solid/liquid phase the following species were considered:

- Dry biomass
- Char
- Moisture

The gas phase contains the following species:

- CO
- CO_2
- H_2O
- H_2
- O_2
- CH_4
- C_2H_4
- Primary tar
- Secondary tar (C_6H_6)
- N_2

$$\frac{\partial(\epsilon_r \rho_g Y_i)}{\partial t} = -\frac{\partial(\rho_g Y_i w_g)}{\partial z} + \dot{r}_i$$

Equation 12: Mass balance equation gas species

$$\epsilon_r \rho_g c_{p,g} \frac{\partial T_g}{\partial t} = -\rho_g c_{p,g} w_g \frac{\partial T_g}{\partial z} + \frac{\partial}{\partial z}\left(\Lambda_g \frac{\partial T_g}{\partial z}\right) - \sum_k \dot{r}_k \Delta h_k + \dot{Q}_{s,g} - \dot{Q}_{g,l}$$

Equation 13: Energy balance equation gas species

$$\frac{\partial((1-\epsilon_r)\rho_s Y_i)}{\partial t} = -\frac{\partial(\rho_s Y_i w_s)}{\partial z} + \dot{r}_i$$

Equation 14: Mass balance equation solid species

$$(1-\epsilon_r)\rho_s c_{p,s} \frac{\partial T_s}{\partial t} = -\rho_s c_{p,s} w_s \frac{\partial T_s}{\partial z} + \frac{\partial}{\partial z}\left(\Lambda_s \frac{\partial T_s}{\partial z}\right) - \sum_k \dot{r}_k \Delta h_k + \dot{Q}_{s,g} - \dot{Q}_{g,l}$$

Equation 15: Energy balance equation solid species

$$v_g = \frac{k_s}{\mu_g}\frac{\partial_p}{\partial_z}$$

Equation 16: Darcy law

$$\rho_g = -\frac{pM_m}{RT_g}$$

Equation 17: Ideal gas equation

The equations 4 to 7 are then spatially integrated to form a system of ordinary differential equations. This system is solved by the *Matlab* routine *ode15s*, which is a multi-step solver and can handle stiff equations.

3.3 Chemical reaction in sub processes

This chapter shows the chemical reaction that happen part in each of the sub processes and the corresponding reaction rates and kinetics.

3.3.1 Chemical reactions

Drying zone

Drying was described by an Arrhenius equation (Equation 18). The chemical reaction is shown in Equation 2.

Pyrolysis zone

The pyrolysis zone is also described by an Arrhenius equation (Equation 19). The solid velocity and the particle size stay the same for this process. Intra-particle gradients are not considered for the simulation. The scheme of the pyrolysis is later explained in the validation chapter. The biomass used in the simulation was softwood (composition shown in Table 4). The chemical reaction is shown in Equation 3.

Softwood composition	
Component	Mass [%]
Cellulose C6H10O5	44
Hemicellulose C5H8O4	26
Lignin C C15H14O4	17.5
Lignin H C22H28O9	9.5
Lignin O C20H22O10	3

Table 4: Softwood composition [4]

The exact yields of each species are shown in the next chapter at the evaluation of the pyrolysis zone. (Table 15)

Tar cracking was implemented in the simulation. Due to the downdraft configuration, the products of the pyrolysis must pass the oxidation zone. There they are exposed to temperatures above 500°C needed for tar cracking [14]. The yields of tar cracking are presented in the validation of the simulation

Oxidation zone

The shrinking core model was used to describe the char conversion. In this model, the bulk density of the bed stays constant while the solid velocity and the particle size are reduced during the conversion. The reduction of the particle volume (Vp) is done as a function of the char conversion (Xchar) and shown in Equation 24. The reduction of the solid velocity is described in Equation 25. For the char conversion reaction rates, the surface kinetics and the external mass transfer limitation - due to diffusion of the reactant to the particle - are also included (see Equation 21, Equation 35, Equation 36). The calculation of the specific particle surface area can be seen in Equation 27. The chemical reaction, which take place in the oxidation zone are shown in Equation 5, Equation 6, Equation 7, and Equation 8.

Gasification zone

The gasification of char coal is described by the shrinking core model, which was also used for the oxidation of charcoal. The chemical reactions are shown in Equation 9, Equation 10 and Equation 11

3.3.2 Reaction rates

Drying zone

$$\dot{r}_{dry} = \rho_s Y_i (1 - \varepsilon_r) A e^{\frac{-E}{RT_s}}$$

Equation 18: Reaction rate drying

Pyrolysis zone

$$\dot{r}_{pyr} = \rho_b A_{pyr} e^{\frac{-E_{pyr}}{RT_s}}$$

Equation 19: Reaction rate pyrolysis

$$\dot{r}_{tcr} = \epsilon_r \rho_t A_{tcr} e^{\frac{-E_{tcr}}{RT_g}}$$

Equation 20: Reaction rate tar cracking

Oxidation and Gasification zone

$$\dot{r}_{gas,O_2} = \frac{A_p M_{m,c} c_g X_{H_2O}}{1/k_k + 1/\beta}$$

Equation 21: Reaction rate char oxidation

$$\beta = \frac{2.06 w_g Re^{-0.575} Sc^{-2/3}}{\epsilon_r}$$

Equation 22: Mass transfer coefficient

$$k_k = A e^{\frac{-E}{RT_s}}$$

Equation 23: k_k factor char reactions

$$V_p = V_{p,0}(1 - X_{char})$$

Equation 24: Reduction solid volume

$$v_s = v_{s,0} \frac{V_p}{V_{p,0}}$$

Equation 25: Reduction of solid velocity

$$\eta = \frac{12\, e^{\frac{-3300}{T_s}}}{1 + 12\, e^{\frac{-3300}{T_s}}}$$

Equation 26: CO/CO_2 ratio

$$A_p = 6\,(1 - \varepsilon_r) / d_p$$

Equation 27: Particle surface area

$$\dot{r}_{gas,H_2O} = \frac{A_p M_{m,c} c_g X_{H_2O}}{1/k_k + 1/\beta}$$

Equation 28: Reaction rate H_2O gasification

$$\dot{r}_{gas,CO_2} = \frac{A_p M_{m,c} c_g X_{CO_2}}{1/k_k + 1/\beta}$$

Equation 29: Reaction rate CO_2 gasification

$$\dot{r}_{wgs} = \epsilon_r M_{m,CO} A_{wgs} e^{\frac{-E_{wgs}}{RT_g}} c_g^2 (X_{CO} X_{H_2O} - X_{CO_2} X_{H_2} / k_{eq,wgs})$$

Equation 30: Reaction rate water gas shift

$$\dot{r}_{ox,CH_4 Dryer-Glasmann} = \epsilon_r M_{m,CH_4} A_{ox,CH_4} e^{\frac{-E_{ox,CH_4}}{RT_g}} c_g^2 X_{CH_4}^{0.7} X_{O_2}^{0.8}$$

Equation 31: Reaction Rate CH_4 Dryer Glasmann

$$\dot{r}_{ox,CH_4 Jones-Lindstedt} = \epsilon_r M_{m,CH_4} A_{ox,CH_4} e^{\frac{-E_{ox,CH_4}}{RT_g}} c_g^2 X_{CH_4}^{0.5} X_{O_2}^{1.25}$$

Equation 32: Reaction rate CH_4 Jones Lindstedt

$$\dot{r}_{ox,CO Jensen} = \epsilon_r M_{m,CO} A_{ox,CO} e^{\frac{-E_{ox,CO}}{RT_g}} c_g^2 X_{CO} X_{O_2}^{0.5} X_{H_2O}^{0.5}$$

Equation 33: Reaction rate CO oxidation

$$\dot{r}_{ox,H_2 GomezBarea} = \epsilon_r M_{m,H_2} A_{ox,H_2} e^{\frac{-E_{ox,H_2}}{RT_g}} c_g^2 X_{H_2} X_{O_2}$$

Equation 34: Reaction rate H_2 oxidation

3.3.3 Reaction kinetics and enthalpies

In literature, there were several models with different kinetics [9] [7] [24] [22] [23] . To find suitable kinetics for the simulation, it was necessary to investigate which kinetics work best and lead to plausible results. The kinetics shown in Table 5 are the ones that were used for simulation, which are later described in this master thesis. Kinetics that were investigated but did not lead to successful simulations are not shown.

Reaction rates kinetics and enthalpies			
Reaction	A	E[kJ/kmol]	Δh [kJ/kg]
Drying	5.56E+6s^{-1} [5]	8.79E+04[5]	2250
Pyrolysis (inert)	2.0E+8s^{-1} [6]	1.33E+06 [6]	-20.95
Pyrolysis (oxidative)	2.0E+8s^{-1} [6]	1.33E+06 [6]	-1730.59
Tar (Liden)	4.26E+6s^{-1}[32]	108 [32]	70.6
Tar (Rath)	3.08E+3s^{-1}[33]	66.3[33]	70.6
Tar (Morf)	4.00E+4s^{-1}[37]	76.6[37]	70.6
Char oxidation	4.75E+3 ms^{-1} [5]	2.003E+05[5]	- 30681 (1 - η) - 9448η
Char gasification V1 CO_2	1.00E+07 ms^{-1}[7]	2.23E+05[7]	12244
Char gasification V2 CO_2	2.00 E+07 ms^{-1}	2.23E+05	12244
Char gasification V1 H_2O	2.00E+07 ms^{-1} [7]	2.23E+05[7]	9153
Char gasification V2 H_2O	4.00E+07 ms^{-1}	2.23E+05	9153
Water gas shift[i] (Bibal)	2.78E+3 $m^6kmol^{-2}s^{-1}$[8]	1.26E+04[8]	-1471
CO oxidation (Jensen)	3.25E+10 s^{-1}[31]	125.6 [31]	-10107
CH_4 oxidation (Jones-Lindstest)	4.40E+11 $(m^{-3}kmol^{-1})^{-0.75}s^{-1}$ [29]	126 [29]	-32450
CH_4 oxidation (Dryer Glassman)	5.01E+11 $(m^{-3}kmol^{-1})^{-0.5}s^{-1}$[30]	200 [30]	-32450
H_2 oxidation (Gomez Barea)	2.20E+09 $m^3kmol^{-1}s^{-1}$ [28]	109 [28]	-120900

Table 5: Reaction rates and enthalpies

3.4 Heat and mass transfer

For the heat and mass transfer the following modes are considered in the model.

Mass transfer

- Solid and gas convection

Heat transfer

- Solid and gas advection
- Solid and gas thermal conduction, based on thermal dispersion coefficients
- Solid to gas heat transfer
- Boundary conditions: Heat release to the lateral, bottom and top of the reactor

The solid thermal dispersion, the thermal conductivity of the bed without flow (λ_{bed}) and the effect of the flow are described by the Peclet number (Equation 35). The gas thermal dispersion is equal to the gas thermal conductivity (Equation 36).
To calculate the thermal conductivity of the bed (λ_{bed}), the following parameters had to be considered according to Tsotsas[15] [16]: radiation, particle shape and porosity of the bed.

$$\Lambda_s = \lambda_{\mathrm{bed}} + \frac{\lambda_g Pe}{2}$$

Equation 35: Solid thermal dispersion

$$\Lambda_g = \lambda_{\mathrm{g}}$$

Equation 36: Gas thermal dispersion

$$Pe = \frac{\mathrm{w}_g c_{p,g} \rho_g d_p}{\lambda_{\mathrm{g}}}$$

Equation 37: Peclet number

The solid to gas heat transfer was modelled after Hobbs [11] and corroborates the results of Cooper and Hallet [12].

$$\dot{Q}_{s,g} = \frac{2.06 c_{p,g} \rho_g w_g Re^{-0.575} Pr^{2/3} A_p (T_s - T_g)}{\epsilon_r}$$

Equation 38: Solid to gas heat transfer

$$A_p = 6\,(1 - \epsilon_r)/d_p$$

Equation 39: Specific surface area

The lateral heat release is calculated with a global α coefficient ($\alpha_{s/g,l}$) which consists of the thermal resistance of the solid/gas to the wall ($\alpha_{s/g,w}$), the insulation between wall and outside (α_{out}) and the thickness and thermal conductivity of the insulation layers. Heat releases at the top and bottom of the reactor are inputs of the model.

$\alpha_{s/g,w}$ is calculated after a model based of Hobbs[11]. α_{out} is based on radiation and natural convection.

$$\dot{Q}_{s/g,l} = \frac{4\ \alpha_{s/g,l}}{d_r}\ (T_{s/g} - T_{amb})$$

Equation 40: Lateral heat loss

$$\frac{1}{\alpha_{s/g,l}} = \frac{1}{\alpha_{s/g,w}} + \sum \frac{\delta_{ins}}{\lambda_{ins}} + \frac{1}{\alpha_{out}}$$

Equation 41: Global α coefficient

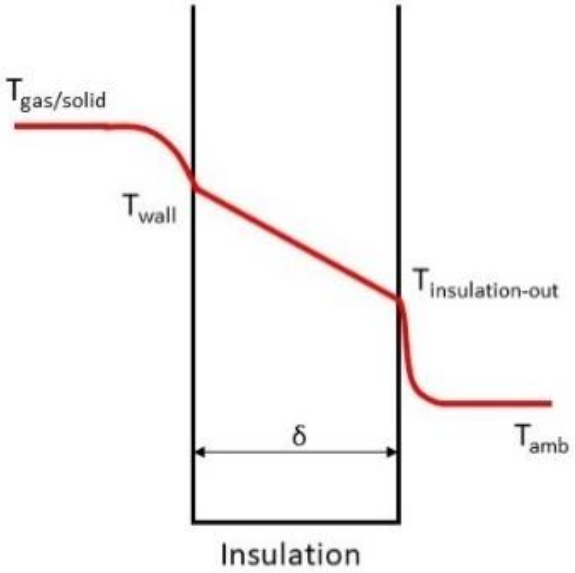

Figure 3: Lateral heat loss

4 EVALUATION OF THE SUB PROCESSES

The issue of the downdraft gasification simulation is complex as the high temperatures in the oxidation zone tend to make the simulations unstable. Furthermore, literature on similar simulations showed that several different kinetics were used for the reactions.
To validate the simulations, it was necessary to compare the results with the experimental data. This data was either provided from literature or from the reactor located at the institute. Due to the complexity of simulating downdraft gasification, the simulation was divided in sub-processes, which were validated with suiting experimental data taken from literature.

4.1 Evaluation of charcoal gasification

The char gasification zone of the reactor is essential for the stability and the efficiency of the process and therefore was the first process, which was validated. The experimental data, which was used for the validation was taken from a paper written by Teixeira, et al.[3].

For the experiment, chips from maritime pinewood were first put in an external pyrolysis reactor to form char coal. The char was added at the top of the reactor via a conveyer belt (a in Figure 4). The gasifying stream is generated by two propane burners (c in Figure 4) and a superheated steam generator (d in Figure 4). The composition of the gasification medium is shown in Table 6. The bed height was maintained constant during the experiment by removing the solid residue at the bottom (e in Figure 4). [3]

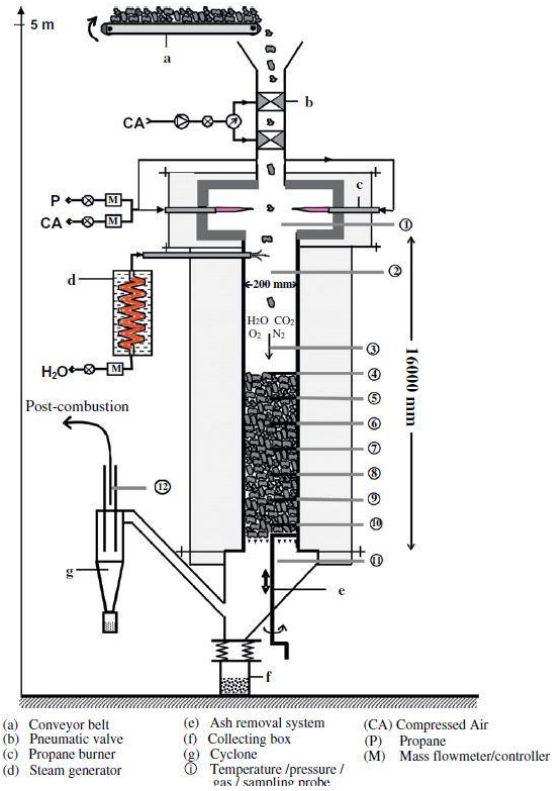

Figure 4: Scheme of char gasification experiment [3]

Operation conditions for the experiment		
Reacting gas	Mol yields [%]	Mol Flow [mol/min]
H_2O	28	3.2
CO_2	8.2	0.9
O_2	2.7	0.3
N_2	61.1	7.0
Solid Char mass flow [g/min]		28
Temperature inlet gas [°C]		1028
Bed height [mm]		650

Table 6: Operation condition char gasification experiment [3]

To validate the char gasification zone, three different sets of reaction kinetics are shown. The first two cases differ in their reaction rates for gasification. The reaction rates which were used for the three gasification simulations are shown in Table 7. The corresponding values for the pre-exponential factor and the activation energy of the reactions are shown in Table 5. The char gasification kinetics for Gas.1 were taken from literature[7]. For Gas. 2 and Gas. 3 the kinetics from literature were adapted by multiplying the pre-exponential factor of the Arrhenius equations by factor 2.
The Gas.3 simulation was done without water gas shift reactions to show its influence (Figure 11).

Kinetics for gasification simulations			
Sim	CO gasification kinetics	H_2O gasification kinetics	Water gas shift kinetics
Gas.1	Char gasification V2 CO_2	Char gasification V2 H_2O	Bibal
Gas.2	Char gasification V1 CO_2	Char gasification V1 H_2O	Bibal
Gas.3	Char gasification V2 CO_2	Char gasification V2 H_2O	-

Table 7: Kinetics for gasification simulations

A more detailed listing of the relevant simulation parameters is shown in Table 8.

Sim	Gas.1	Gas.2	Gas.3
Mass in Gas [kg/h]	19.71	19.71	19.71
Mass in Solid [kg/h]	1.68	1.68	1.68
MOIST_IN [-]	0	0	0
NGRID_REACTOR	40 [1;1;1;1;3]	40 [1;1;1;1;3]	40 [1;1;1;1;3]
NRXN	13	13	13
tstop [s]	800	800	800
tsave [s]	100	100	100
deltat [s]	50	50	50
POROSITY_REACTOR [-]	0.74	0.74	0.74
R_PART_0 [-]	0.005	0.005	0.005
R_REACTOR [m]	0.1	0.1	0.1

L_REACTOR [m]	0.65	0.65	0.65
Pyrolysis	Inert	Inert	Inert
Solid fuel	Charcoal	Charcoal	Charcoal
Y_GAS_IN	H2O: 19.02%; CO2: 13.08% O2: 3.17%; N2: 64.73%	H2O: 19.02%; CO2: 13.08% O2: 3.17%; N2: 64.73%	H2O: 19.02%; CO2: 13.08% O2: 3.17%; N2: 64.73%
F_GAS	2	1	2
LAMBDA_INS [W/(mK)]	0.1	0.1	0.1
L_INS [m]	0.15	0.15	0.15
E_LOSS_TOP [W/m²]	-30500	-30500	-30500
E_LOSS_DOWN [W/m²]	1000	1000	1000
TH._CON.WOOD [W/(mK)]	0.17	0.17	0.17
Temperature fire stone	-	-	-
T_IN_G[K]	1300	1300	1300
T_IN_SOLID[K]	300	300	300
Water gas shift	Biba	Biba	-
Gas phase oxi. reaction			
CO	-	-	-
H2	-	-	-
CH4	-	-	-
Tar Cracking		-	-
Primary	-	-	-
Secondary	-	-	-

Table 8: Relevant input data for gasification simulation

4.2 Evaluation of charcoal gasification results

The following diagrams show the simulation Gas.1, except for Figure 11, where a comparison between Gas. 1 and Gas 3. Is shown.
The charcoal enters the reactor at 0.65 m (right side of the diagram) and the producer gas escapes at 0m (left side). All diagrams are shown in a steady state.

4.2.1 Diagrams for charcoal gasification

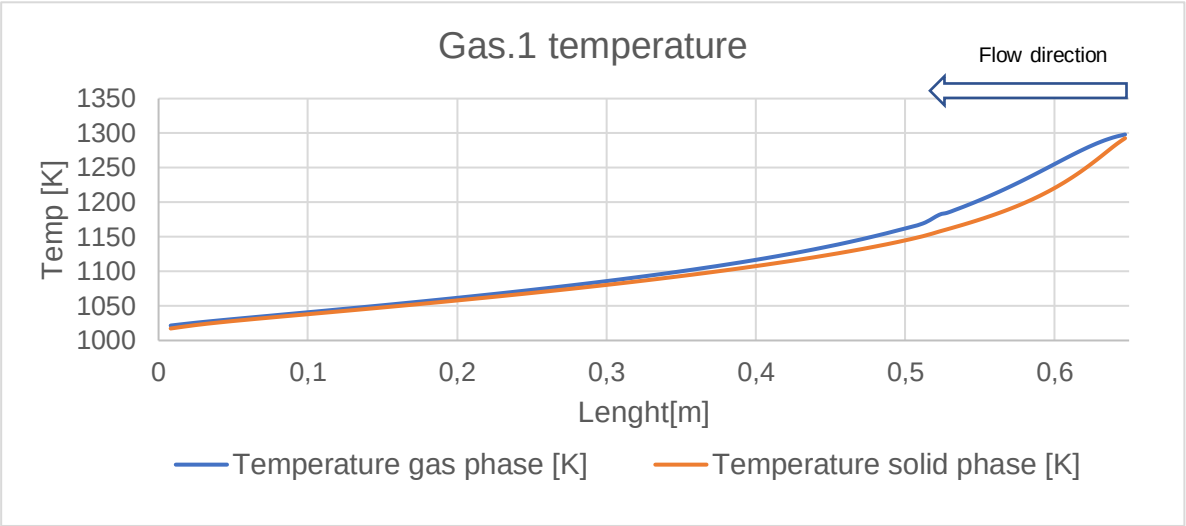

Figure 5: Temperature Gas.1 simulation

In the diagram below the mol yields of the charcoal gasification are depicted (the nitrogen yields are cut of in this diagram). The processes, which can be seen in this diagram, are oxidation and gasification of charcoal and the water gas shift.

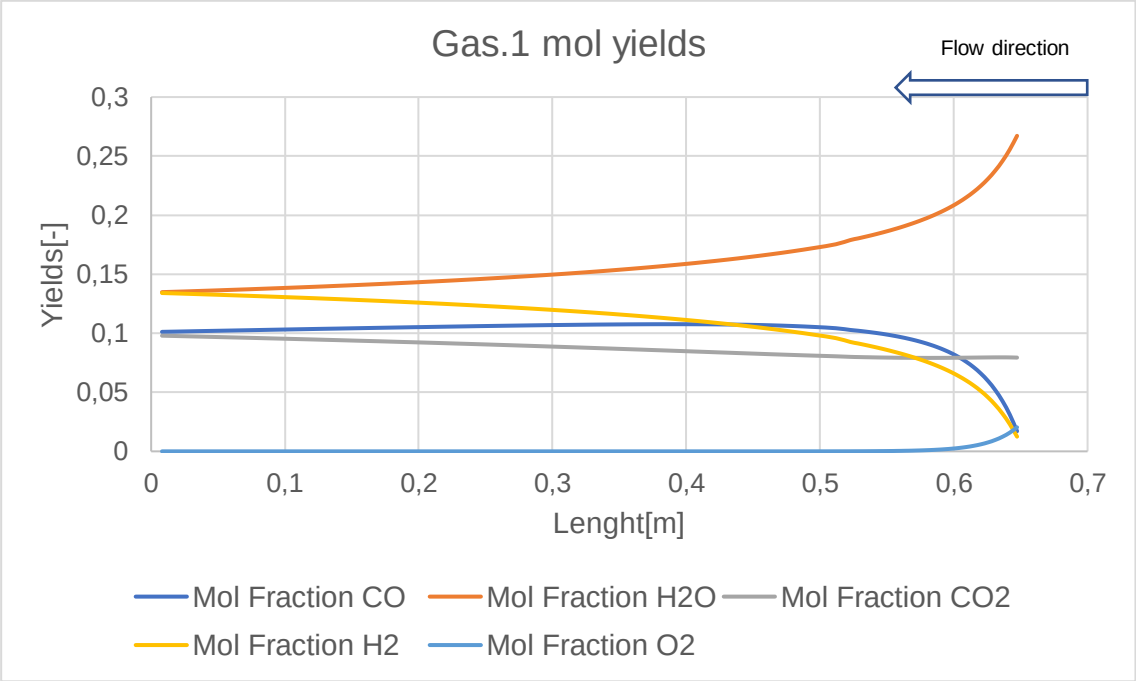

Figure 6: Mol yields Gas. 1 simulation

Figure 7 shows the mass flow of charcoal. Notably, most charcoal is consumed between 0.5 and 0.65 m, where oxygen is available, and the temperatures are at the highest value.

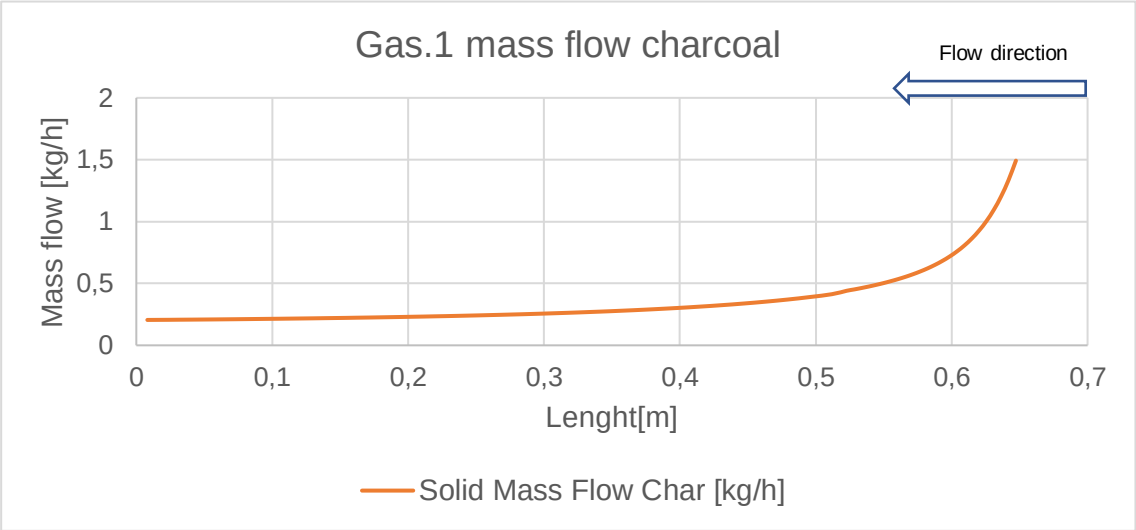

Figure 7: Mass flow charcoal Gas. 1 simulation

For the charcoal gasification experiment of Teixeira [3][1], diagrams for the molar yields and temperatures along the reactor available, the next diagrams show this comparison.

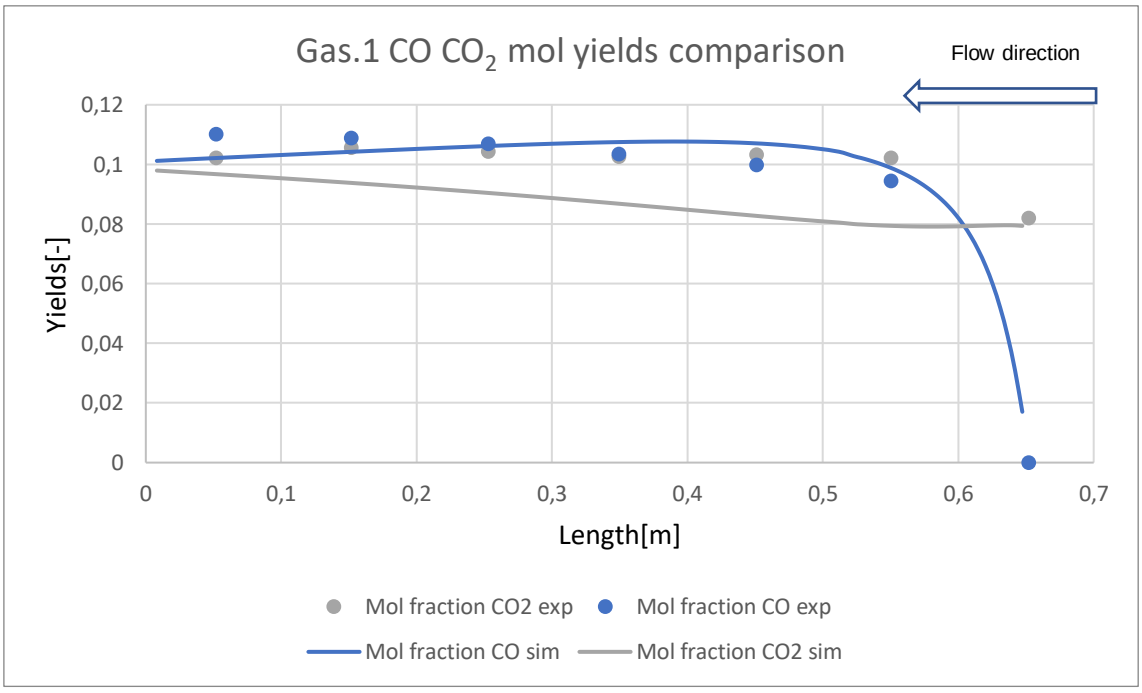

Figure 8: CO CO_2 mol yields comparison between experimental data and Gas.1 simulation

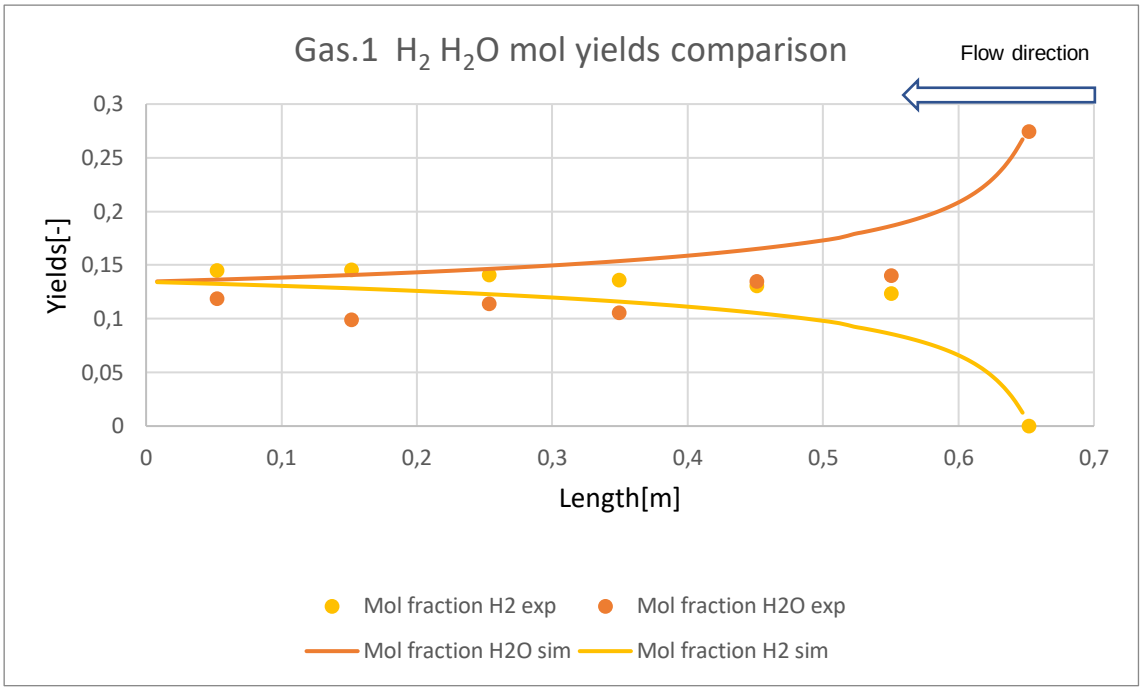

Figure 9: H_2 H_2O mol yields comparison between experimental data and Gas.1 simulation

In Figure 10 the comparison of the solid phase temperatures between the experiment and the simulation is shown. The heat losses at the bottom, the top, and the lateral heat release were determined by comparing the experiment to the simulation and adjusting the values (see Table 9). At the top, there is a positive heat transfer, which is caused by the radiation of the hot gas. At the bottom, there is very little heat loss. The lateral heat release was adjusted by the thickness and thermal conductivity of the assumed insulation layers.

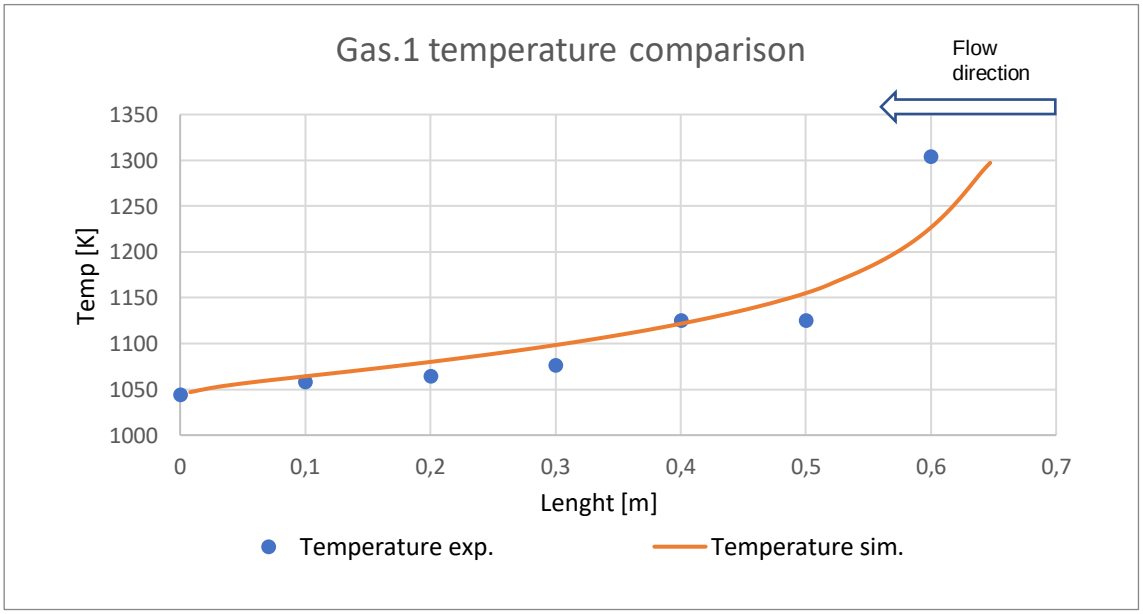

Figure 10: Temperature comparison between experimental data and Gas.1 simulation

Heat release gasification	
Heat release top [kW]	-0.9582
Heat release bottom [kW]	0.0314
Lateral heat release [kW]	0.6710
λ [W/(mK)]	0.1
L [m]	0.15

Table 9: Heat release gasification

Figure 11 shows the difference between the simulations with and without water gas shift. The dotted lines show the molar yields without water gas shift while the whole lines depict the simulation with the Biba water gas shift reactions. A significant difference can be seen between these two simulations. The yields of H_2O and CO were reduced while the yields of CO_2 and H_2 increased. The chemical reaction for the water gas shift is described in Equation 11.

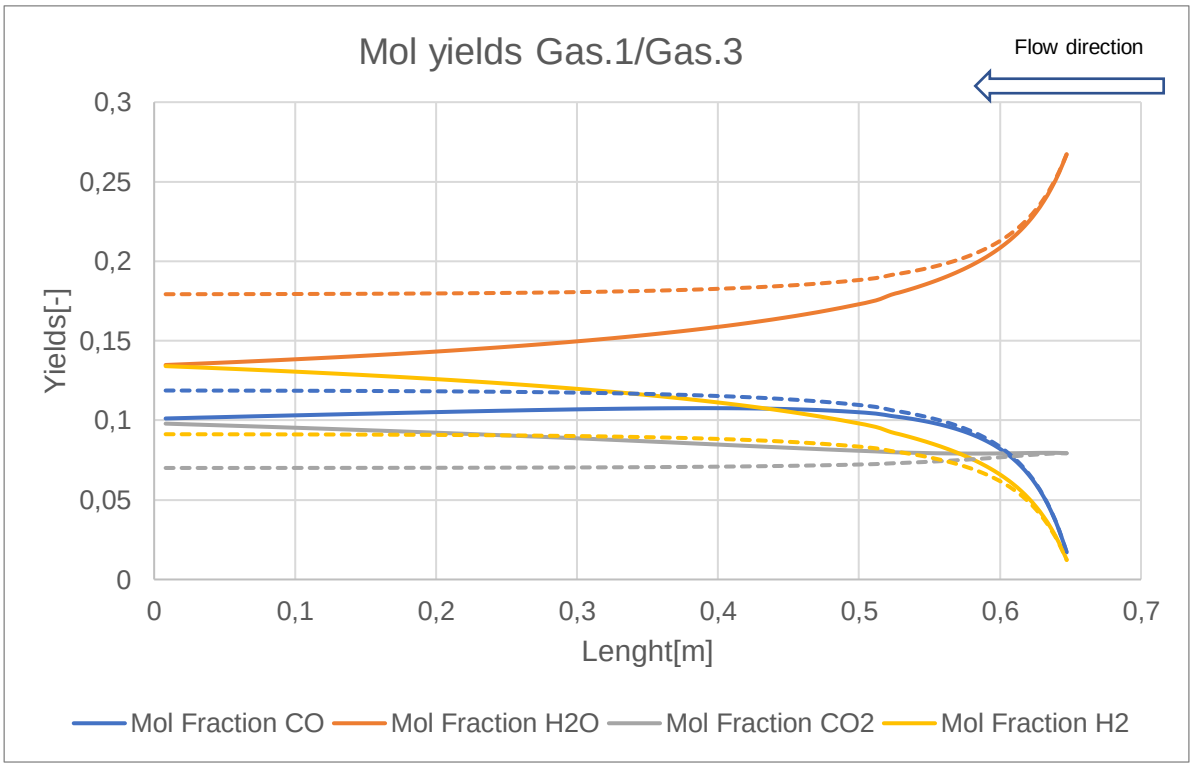

Figure 11: Mol yield comparison Gas1 Gas.3 simulations

4.2.2 Discussion results

The best results were achieved in the simulation Gas.1 for this simulation the adapted kinetics for gasification were used, which are faster than the kinetics used for Gas.2. Therefore, the yields of CO and H_2 are higher for Gas.1 than for Gas.2. Gas.1 had also the water gas shift reactions of Biba [8] implemented. To show the influence of the water-gas-shift reactions, the simulation Gas.3 was done without them. The impact can be seen in Figure 11 and in Table 10.

Table 10 demonstrates the comparison between the experimental data and the simulation data. Like it was mentioned before simulation Gas.1 shows the best results compared to the experimental data.

The char gasification zone of the simulations is now well described and validated. The results gained from this chapter will be used for the next simulations in the later chapters.

Mol yields [%]	Experiment	Gas.1	Gas.2	Gas.3
CO	11.02%	10.89%	10.23%	11.76%
H_2O	10.21%	13.16%	14.21%	18.05%
CO_2	12.02%	9.45%	9.45%	7.03%
H_2	14.52%	13.67%	12.72%	9.03%
N_2	52.35%	52.85%	53.39%	54.13%
Dry solid unconverted mass	~10%	9.56%	15.84%	24.59%
Mass error		0.08%	0.12%	0.21%
Enthalpy error		0.76%	1.12%	1.96%

Table 10: Yields comparison experiment/simulations

The energy and mass balances are well closed in general. Minor errors for enthalpy occur because the equations are not written conservatively, and temperature-dependent enthalpies were assumed to be constant.
For further validation of the simulation, the atom balances from the input and the output were compared; The values should coincide. The input consists of the gasification agent, the solid fuel and moisture. The output consists of the producer gas and the solid unconverted mass. Table 11 shows the atom balances for the Gas.1 simulation, for which differences are also minor.

Atom balances gasification				
	C	H	O	N
Input Mass	10.44%	2.185%	27.72%	59.64%
Output Mass	10.61%	2.185%	27.67%	59.52%
Difference	-0.1738%	-8.792E-05%	0.04829%	0.1256%

Table 11: Atom balances gasification

4.3 Evaluation of pyrolysis and oxidation zone

The stability of the oxidation zone is particularly interesting for operators. Because of the low temperatures, which occur at the top of the reactor, the reduction of tar is controlled by the oxidation zone, were high temperatures occur. The pyrolysis zone is important for the stability of the system as well. Partial oxidation in the pyrolysis zone can provide energy for the drying and heating zone, which allows the process to be autothermal.[9]

The reactor used for this experiment and in the gasification experiments is the same. The experiments that were taken into consideration were conducted by Daouk et al.[9]. In this experiment, biomass was gasified with air. The reactor here is a continuous fixed bed downdraft gasifier. Every 10 cm, the reactor has thermoelements mounted along its length (T1 -T9 in Figure 12). At the reactor´s lower part, a sampling pipe is located to collect gases at the outlet. Biomass is provided by a conveyer belt and enters the reactor at the top. Two pneumatic valves serve as an airlock (2 in Figure 12). The char is removed manually at the bottom of the reactor. Air is heated in the air preheater (10 in Figure 12) and is then injected at the top of the reactor. The reactor operates at a low air-fuel ratio (λ = 0.11). The operation conditions for the experiment are shown in Table 8. [9]

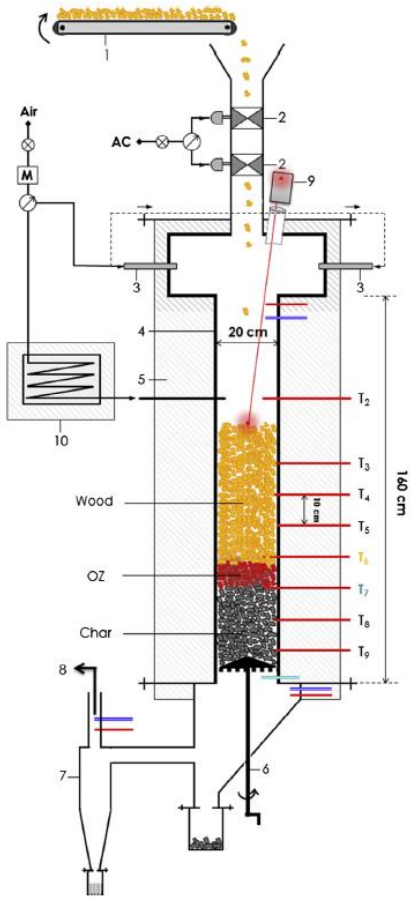

Figure 12: Reactor for Daouk et al. [9] experiments

The operating conditions for this experiment are demonstrated in Table 12.

Operation conditions for the experiment	
Reacting gas	
O_2 [Mass%]	23.135
N_2 [Mass%]	76.865
Woodchips mass flow [kg/h]	2.63
Air mass flow [kg/h]	3.72
Temperature inlet gas [K]	400
Bed height [mm]	0.7

Table 12: Operation conditions for Daouk experiment

The experiments of Daouk et al. [9] were used to validate the pyrolysis and the oxidation zone. Just as for the validation of the gasification zone, various kinetics to describe the reactions could be found in literature. Only attempts that turned out to be successful are presented in this master thesis. Moreover, only a selection of three different sets of kinetics is discussed to demonstrate the building method for the model.

Table 13 shows which kinetics had been varied for the simulations (the values for the reaction rates are shown in Table 7). The three reactions which were validated in this stage of simulation were the oxidation reactions in the gas phase (CO, H_2, CH_4), the pyrolysis and the cracking of the primary tars. [9]

Kinetics for Daouk simulations					
Sim	Pyrolysis	CO	H_2	CH_4	Primary tar cracking
Daouk1	Oxidative pyrolysis	Jensen	Gomez Barea	Jones-Lindstedt	Liden
Daouk2	Oxidative pyrolysis	Jensen	Gomez Barea	Gomez Barea	Liden
Daouk3	Oxidative pyrolysis	Jensen	Gomez Barea	Jones-Lindstedt	Rath

Table 13: Kinetics for Daouk simulations

Table 14 shows the relevant input data for the two simulation of the Daouk experiment. The difference between Daouk 1 and Daouk 2 are the kinetics of CH_4 oxidation which is faster in 1. The difference between Daouk 1 and Daouk 3 are the reaction kinetics of the primary tar cracking. Only a selection of the successful simulations is shown in this master thesis.

Sim	Daouk 1	Daouk 2	Daouk 3
Mass in Gas [kg/h]	3.72	3.72	3.72
Mass in Solid [kg/h]	2.63	2.63	2.63
MOIST_IN	0.098	0.098	0.098
NGRID_REACTOR	40 [1;1;1;1;1;1]	40 [1;1;1;1;1;1]	40 [1;1;1;1;1;1]
NRXN	13	13	13
tstop	10000	10000	10000

tsave	50	50	50
deltat	2	2	2
POROSITY_REACTOR	0.6	0.6	0.6
R_PART_0	0.005	0.005	0.005
R_REACTOR	0.1	0.1	0.1
L_REACTOR	0.7	0.7	0.7
Pyrolysis	Oxidative	Oxidative	Oxidative
Mass _In	Biomass	Biomass	Biomass
Y_GAS_IN	Air	Air	Air
F_GAS	1	1	1
LAMBDA_INS	0.1	0.1	0.1
L_INS	0.015	0.015	0.015
E_LOSS_TOP	-	-	-
E_LOSS_DOWN	1000	1000	1000
THERM_CONDUC_WOOD	0.2	0.2	0.2
Temperature fire stone	-	-	-
T_IN_G[K]	400	400	400
T_IN_SOLID[K]	300	300	300
Water gas shift	-	-	-
Gas phase oxidation reaction			
CO	Jensen	Jensen	Jensen
H2	Gomez Barea I	Gomez Barea I	Gomez Barea I
CH4	Jones-Lindstest	Dryer Glassman	Jones-Lindstest
Tar Cracking			
Primary	Liden	Liden	Rath
Secondary	-	-	-

Table 14: Relevant input data for Daouk simulations

4.3.1 Validation of pyrolysis

It was mentioned before that the pyrolysis reactions are important for the stability of the whole process. For the Dauok experiments the gasification agent - in this case air - was introduced at the top of the gasifier and passed the pyrolysis zone. That is also the case for the experiments taken at the institute, which were simulated later.
The oxygen in the pyrolysis zone can lead to partial oxidation of biomass. Providing energy for the heating and drying stage. Therefore, the process is autothermal.

The first simulations were done with an inert pyrolysis scheme. However, this has led to unstable simulations, which often went extinct. The oxidative pyrolysis schemes helped to stabilize the simulations. One reason for these more stable simulations is the extra heat provided by the oxidative pyrolysis. The second reason is that less oxygen is available in later gasification stages because a part of the oxygen is used for the pyrolysis. Another problem for inert pyrolysis was that higher oxygen amount in the oxidation zone led to too much char oxidation, which further led to negative yields of charcoal. Consequently, the simulation crashed.

Two different pyrolysis schemes were used for the simulations. The inert pyrolysis scheme is based on a detailed pyrolysis scheme [17], [18]. The product composition (shown in Table 15) of the inert scheme is obtained with typical conditions in fixed bed conversion, regarding charring and heating rates, for temperatures till the point where char conversion starts.

The oxidative pyrolysis scheme was adapted from the inert scheme. The products of this pyrolysis scheme are also shown in Table 15.

The product gas composition is based on the one from inert conditions. It is then assumed that O_2 reacts to 40% with CO, 40% with CH_4 and 20% to H_2, as well as 25% of tars react with previously introduced tar cracking reaction, to balance the loss of the combustible gases. This distribution was selected based on experimental product compositions for oxidative pyrolysis [35].

The selected parameter, including the oxygen consumption in the reaction, were chosen to obtain an enthalpy of oxidative pyrolysis, which is consistent with measured data [34].

Pyrolysis		
	Pyrolysis yields	Oxidative pyrolysis yields
CO [-]	0.082101	0.086510496
H_2O [-]	0.11412	0.17187
CO_2 [-]	0.1243	0.262695607
H_2 [-]	0.005666	0.005078437
O_2 [-]	-	-0.11
CH_4 [-]	0.016487	0.014794957
C_2H_4 [-]	0.013084	0.013084
C_6H_6 [-]	-	0.013673414
Tar [-]	0.4106789	0.308009175
N_2 [-]	-	-
Softwood [-]	-1	-1
Char [-]	0.23355907	0.23355907
Mass balance	-4.03E-06	-0.000724842
Reaction enthalpy [kJ/kg]	-20.95024786	-1730.589367

Table 15: Pyrolysis schemes

4.3.2 Validation of gas phase oxidation

It is essential to consider and implement the gas phase reactions for the simulations. Firstly, they influence the product yields for the producer gas. Secondly, they also provide additional heat for the process, which helps keeping it autothermal. The gas phase reactions considered are CO, H2, and CH4 oxidation.

To validate the gas phase kinetics, several reaction rates were tested. The results of the producer gas component yield for the simulation were compared to the experimental data afterward.

Table 13 shows the chosen reaction enthalpies for the simulation. To show the process of finding the right kinetics a comparison between two different CH_4 kinetics is shown in the two following simulations (Figure 21). A similar process was used for finding the reaction rates for CO and H_2. The difference between the producer gas yields for the different CH_4 reaction rates is shown in Figure 21.
Figure 13 shows the Arrhenius plot of the CH_4 oxidation reactions. The x-axis shown the temperature (1000/ temperature for better visualisation) and the y-axis shows the reaction rate.

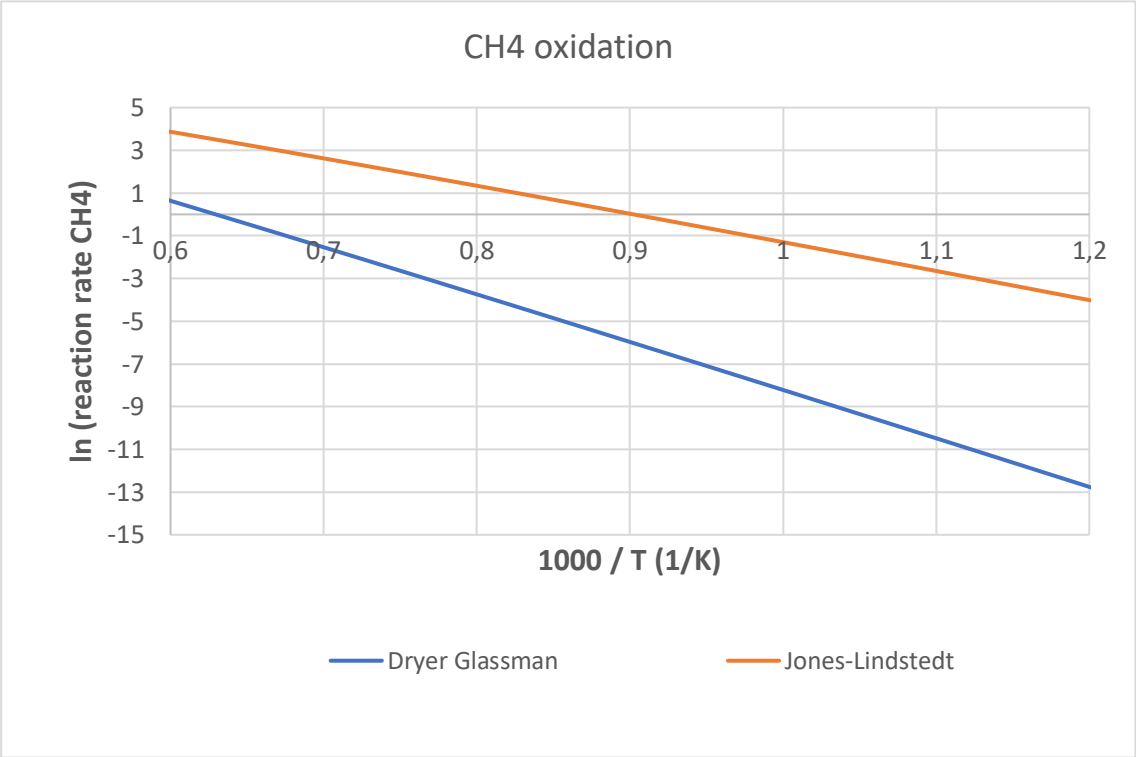

Figure 13: Arrhenius plot CH4 kinetic rates

0.6 on the x-axis equals 1400°C and 1.2 equals 550°C.

4.3.3 Validation of primary tar cracking

To use a downdraft gasifier for a CHP cycle with an internal combustion piston engine the tar content must be minimal. That is described in the simulation by adding tar cracking reactions. For the Daouk simulations, primary tar cracking was added.

The yields of the primary tar cracking products are shown in Table 16. This is based on data from literature[17] but with small adaptations. C_6H_6 is used as a secondary tar species instead of soot. For the simulation different reaction kinetics for the tar cracking were tested (shown in Table 13) and then validated by comparing the producer gas yields with the experimental data. The secondary tar cracking is described in the next chapter.

The difference between the tar cracking kinetics is shown in Figure 20.

Primary tar cracking	
Yields	
CO [-]	0.542933464
H_2O [-]	-
CO_2 [-]	0.169432685
H_2 [-]	0.028082765
O_2 [-]	-
CH_4 [-]	0.126372444
C_2H_4 [-]	-
C_6H_6 [-]	0.133178641
Tar [-]	-1
N_2 [-]	-
Reaction enthalpy [kJ/kg]	-349.03

Table 16: Tar cracking yields

4.4 Evaluation of Daouk experiment

In this chapter, all diagrams that do not present a comparison depict simulation Daouk 3. Biomass enters the reactor at 0.7m and the producer gas exits at 0m. The direction of the flow is indicated by the arrow. All diagrams show a steady state.

.

4.4.1 Diagrams for Daouk experiment

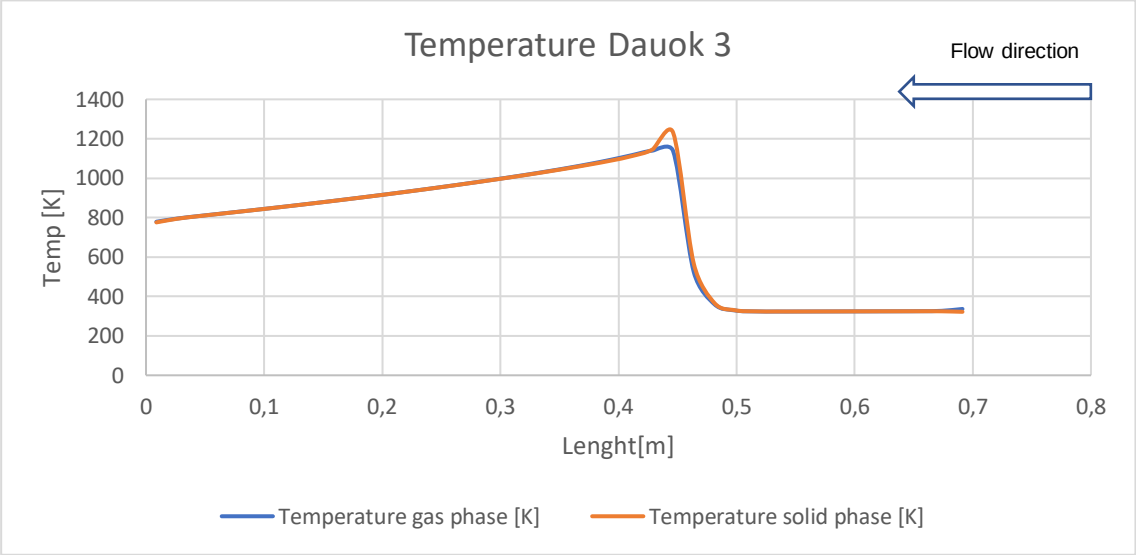

Figure 14: Temperature Daouk 3 simulation

Figure 15 shows the mol yields the right side marks the entrance of the air and the wood chips, on the left side the producer gas leaves. The pyrolysis takes place at around 0.45m and shortly after the oxidation reactions take place. Then CO and H_2 are produced through gasification and the cracking of primary tars.

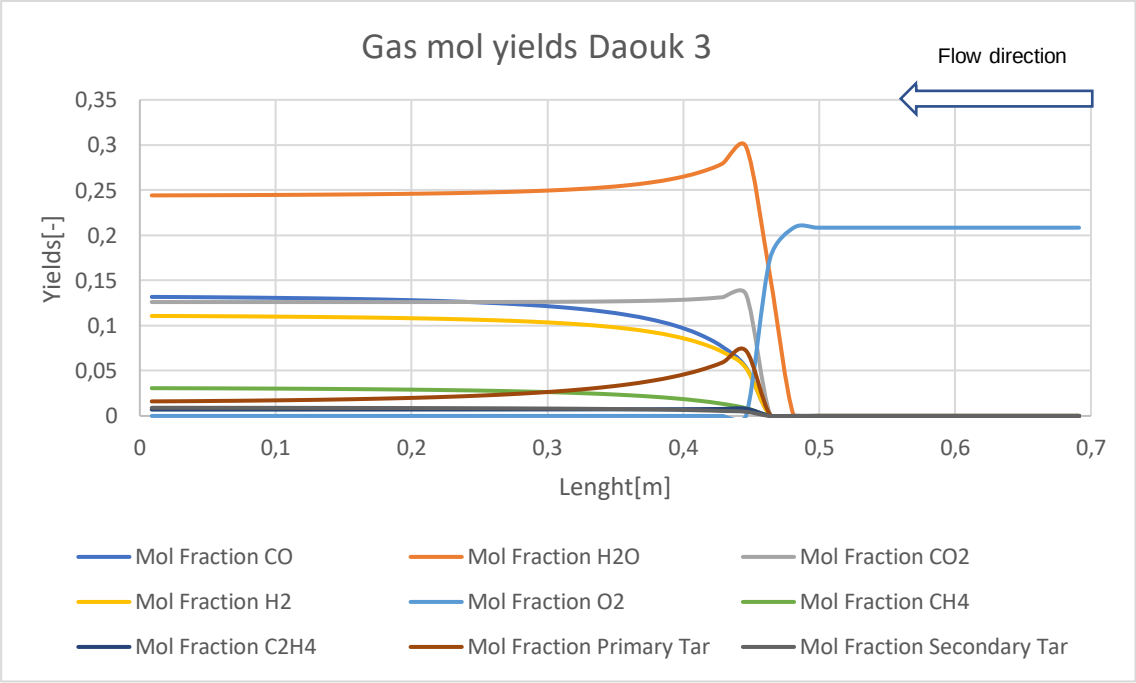

Figure 15: Mol yields Daouk 3 simulation

In Figure 16 it is visible that a lot of the charcoal stays unconverted, the reason for this is that the low amount of air for the experiment and therefore, there is no oxygen left for the oxidation of the charcoal.

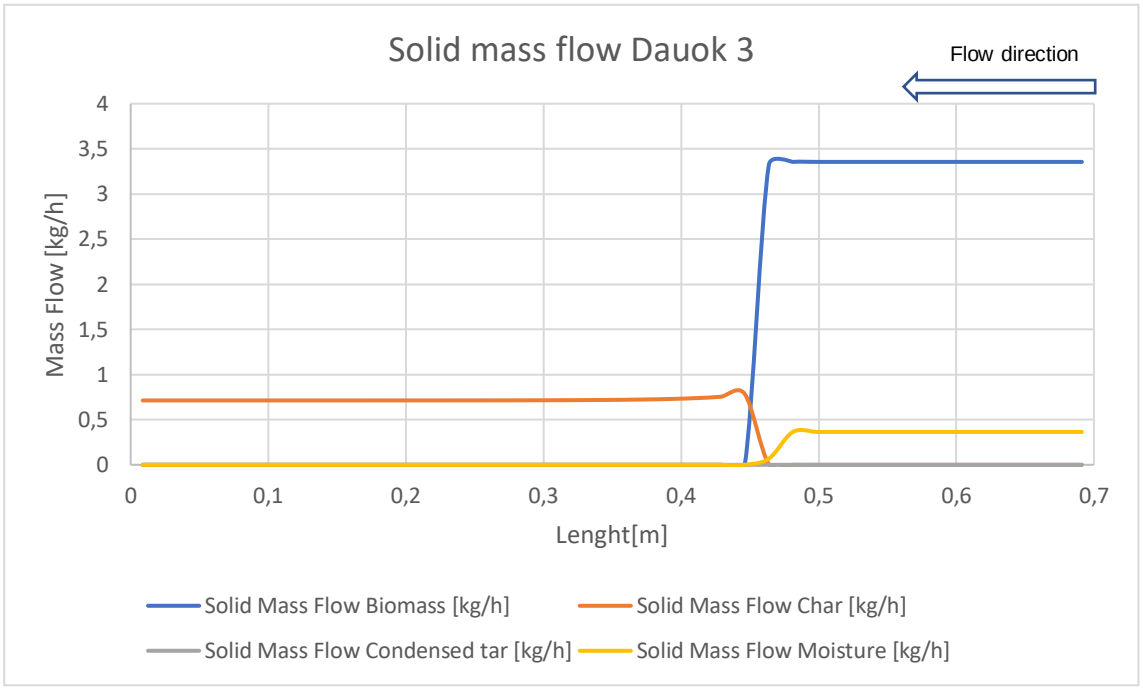

Figure 16: Solid mass flow Daouk 3 simulation

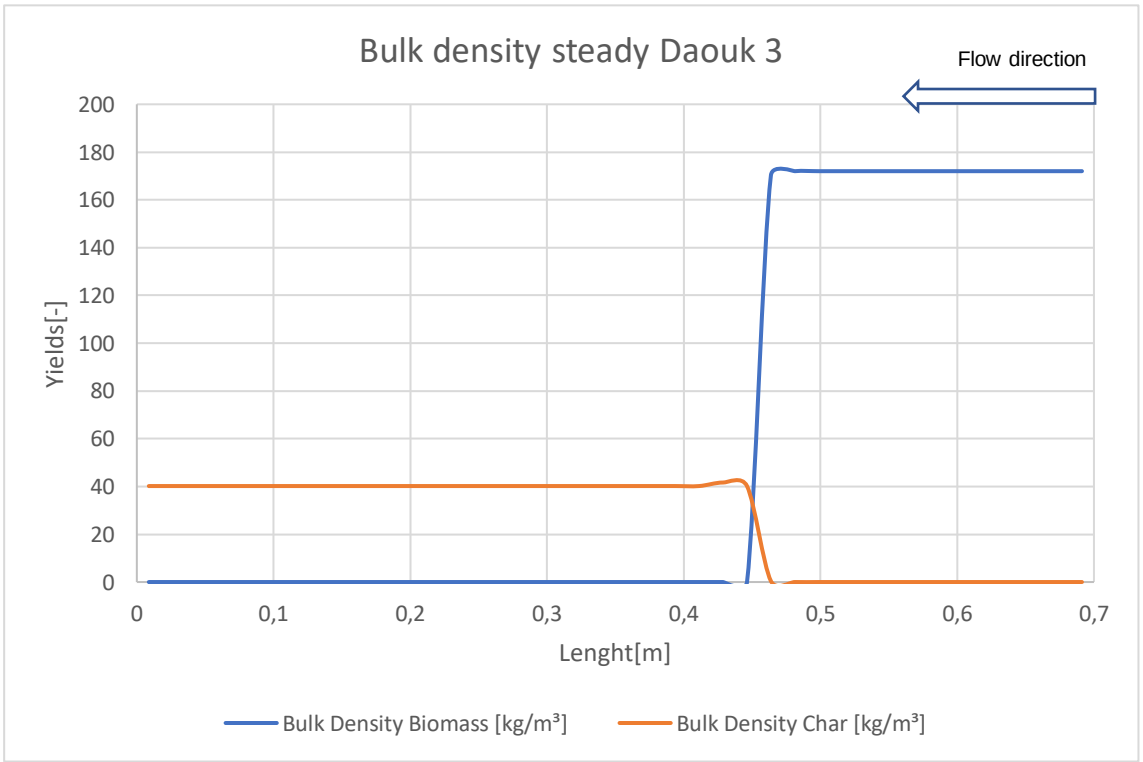

Figure 17: Bulk density Daouk 3 simulation

Figure 19 demonstrates a comparison between the temperatures of the simulation and the experiment. This figure further shows the oxidation front location marked by the peak of the temperatures. The difference is roughly 0.05m, which is acceptable. The temperature at 0.5 m has a high standard deviation because it tends to be in- or outside the oxidation zone. For this diagram, the average temperatures, measured with the sensor inside the oxidation zone, were taken.
This is shown in Figure 18(T6). Figure 19 shows the average temperatures in the reactor over its length from the experiment compared to the simulation.

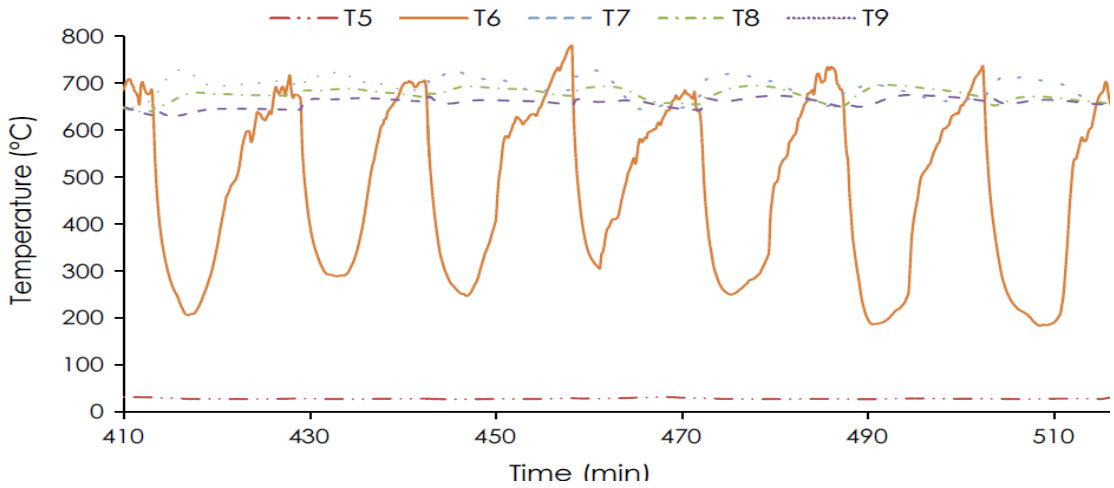

Figure 18: Temperature data over time Daouk et al. experiment [9]

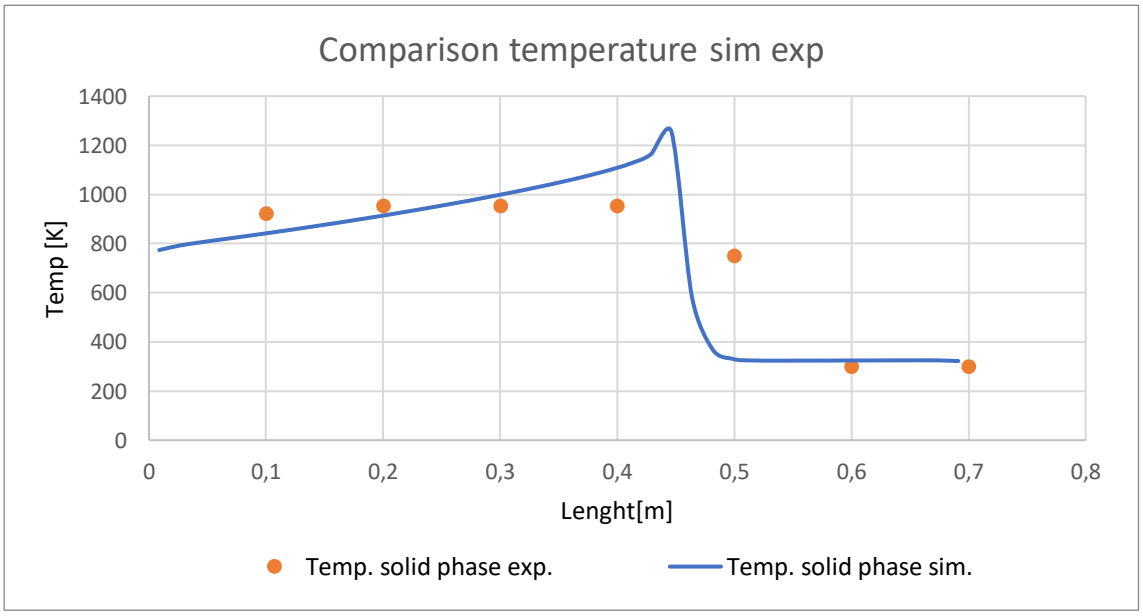

Figure 19: Comparison temperature between experiment and Daouk 3 simulation.

Heat release Daouk	
Heat release top [kW]	0.0
Heat release bottom [kW]	0.0314
Lateral heat release [kW]	1.0794
λ [W/(mK)]	0.1
L [m]	0.015

Table 17: Heat release Daouk

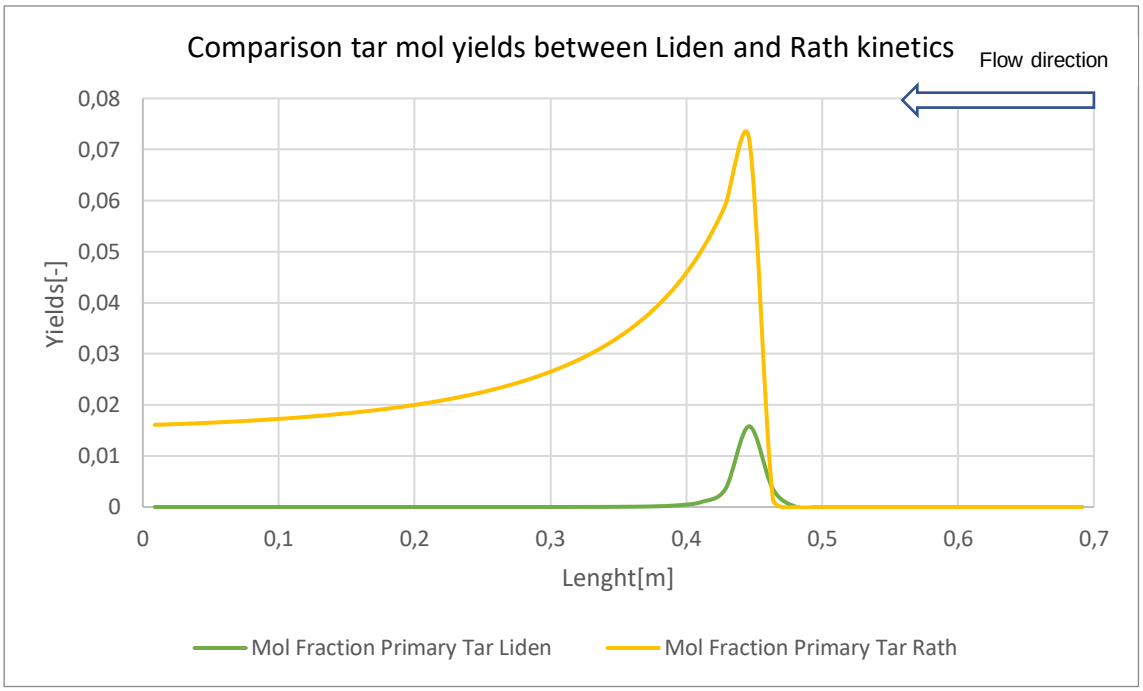

Figure 20: Comparison tar cracking rates between Liden (sim. Daouk 1) and Rath (sim. Daouk 3)

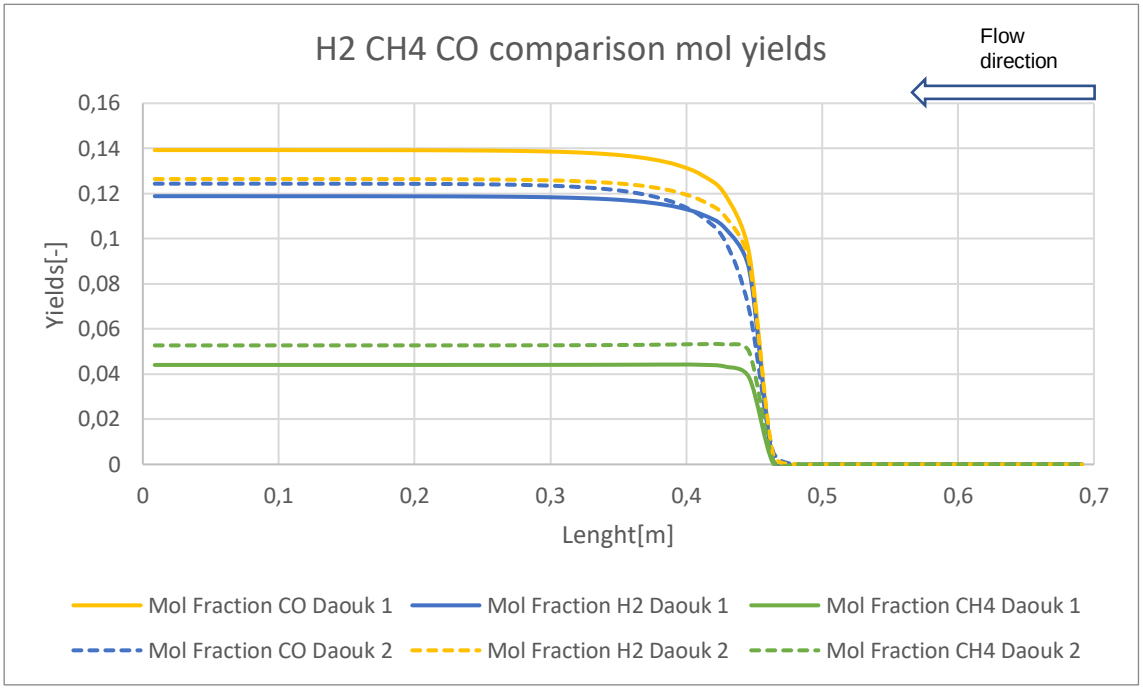

Figure 21: Gas phase yield comparison between Daouk 1 and Daouk 2

4.4.2 Discussion results Daouk

Table 18 presents the comparison between the yields for the three different simulation. The simulations with the most accurate results was Daouk 3. The bigger mass error of the Daouk 2 simulations can be explained by the oxidation front´s tendency to wander towards the top due to the not suiting kinetics for CH_4 oxidation.

Mass yields [%]	Experiment	Daouk 1	Daouk 2	Daouk 3
CO	14.06	15.73	13.94	14.57
H2O	20.42	16.67	15.17	17.35
CO2	19.60	23.79	26.94	21.91
H2	0.78	0.96	1.01	0.87
O2		0.00	0.00	0.00
CH4	1.88	2.84	3.38	1.94
C2H4	0.67	0.78	0.78	0.78
Prim. tar	-	0.00	0.00	3.94
Sec. tar	-	3.47	3.48	2.79
N2	37.15	35.75	35.30	35.85
Tars	5.46	3.46	3.37	6.73
Dry solid unconverted mass [%]	17.23	20.82	19.94	21.25
Mass error [%]		0.05	0.74	0.04
Enthalpy [%]		2.14	3.02	1.82

Table 18: Producer gas yield comparison Daouk

The simulations for the Daouk experiments revealed that an oxidative pyrolysis is necessary for stable simulations. The reasons are that the exothermic reaction of the oxidative pyrolysis provides heat, which is needed in the heating and drying zone. Moreover, the oxidative pyrolysis helps limiting the amount of oxygen for the oxidation zone, which further helps stabilizing the simulation.

For the gas phase oxidation reactions, several reaction rates taken from literature were validated with the experimental producer gas yield composition. To demonstrate the process that was used to find the right kinetics, a comparison between the simulations Daouk 1 and Daouk 2 is depicted in Figure 21. It becomes apparent that due to the faster kinetics for the CH4 oxidation reactions in the simulation Daouk1, less oxygen is available for the oxidation of the other combustible gases. The CO amount is, therefore, higher in the Dauok 1 simulation compared to Dauok 2. The CO_2 amount is lower for the Daouk 1 simulation compared to the Daouk 2 simulation. Therefore, the oxidation reactions of Daouk 1 and 3 were decided on for further simulations.

Two different types of tar cracking kinetics are shown in this master thesis. A comparison between these two is shown in Figure 20. For the Daouk simulations the slower kinetics for tar cracking (Rath) fit better. These were used in the simulation Daouk 3.

The Daouk simulations were first tried with the same lateral heat release like the gasification simulations. These lead to stability issues for the simulations due to more heat of the now oxidative pyrolysis forcing the oxidation front to move upwards. To counter this the lateral heat release was increased, by the reduction of the isolation thickness Table 17.

The pyrolysis and the oxidation zone are now validated and the lessons which were learnt in this chapter can now be used for the final simulation in the next chapter.

Like in the previous simulation the energy and the enthalpy balances are closing. The minor error in the enthalpy has the same causes as discussed before.
For the Daouk Simulations the atom balances were also compared. The table shows the balances for the Daouk 3 simulations (Table 19).

Atom balances Daouk simulation				
	C	H	O	N
Input Mass %	26.9385383	3.81667503	37.4093584	31.8354282
Output Mass %	26.9913598	3.79223478	37.3936632	31.8227422
Difference	-0.05282144	0.02444024	0.0156952	0.01268599

Table 19: Atom balances Daouk 3 simulation

5 EVALUATION OF THE WHOLE PROCESS

To evaluate the whole process, experimental data was taken from the gasifier at the institute that was provided by an industrial partner. The kinetics and parameters were taken from the sub-processes. The simulation was expanded with secondary tar cracking reactions.

The reactor, used for the experiments is a commercially available 85 kW throated downdraft gasifier. As a gasification medium air was used. It enters the gasifier at the top. Wood pellets are the chosen fuel for these experiments and are added at the top as well. At the bottom of the reactor, ashes are removed by a screw conveyer.
A detailed set up for the experiment is described in a paper by Zachl et al. Usually, the product gas escapes at the bottom and flows through a series of heat exchangers and gas filters before it is burnt in an internal combustion engine. The experimental set up at the institute does not have a combustion engine. The producer gas is simply burnt instead.

In the experiments, which were used for the validation, the wood pellets were gasified at an air-fuel ratio of 0.28. The operation conditions for the case, which was validated is shown in

Operation conditions for the experiment		
Reacting gas	Hargassner 1, 2, 3, 4	Hargassner recirculation
O2 [Mass%]	23.135	18.49
N2 [Mass%]	76.865	75.77
CO2 [Mass%]	-	5.74
Woodchips mass flow [kg/h]	18.49	16.06
Air mass flow [kg/h]	32.8	35.54
Temperature inlet gas [K]	300	300
Bed height [mm]	0.36	0.36

Table 20. Two experiments were used for the validation. The simulations Hargassner 1-4 show the gasification with air. The simulation Hargassner recirculation is based on an experiment, where the gasification agent consists of a mixture of CO_2 and air. This experiment should simulate the recirculation of exhaust gases.

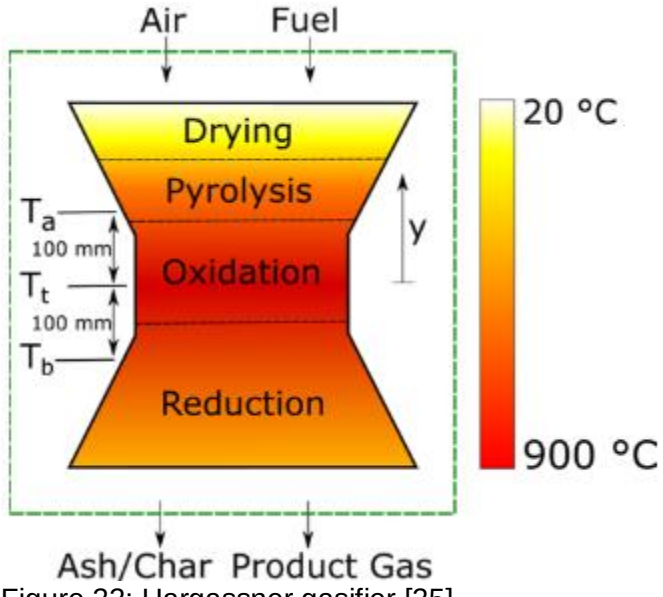

Figure 22: Hargassner gasifier [25]

Operation conditions for the experiment		
Reacting gas	Hargassner 1, 2, 3, 4	Hargassner recirculation
O_2 [Mass%]	23.135	18.49
N_2 [Mass%]	76.865	75.77
CO_2 [Mass%]	-	5.74
Woodchips mass flow [kg/h]	18.49	16.06
Air mass flow [kg/h]	32.8	35.54
Temperature inlet gas [K]	300	300
Bed height [mm]	0.36	0.36

Table 20: Operation condition for experiment

Difference in kinetics for Hargassner simulation		
Sim	CO gasification kinetics	H_2O gasification kinetics
Harg.1	Char gasification V1 CO_2	Char gasification V1 H_2O
Harg.2, 3, 4	Char gasification V2 CO_2	Char gasification V2 H_2O
Harg. Gas.	Char gasification V2 CO_2	Char gasification V2 H_2O

Table 21: Difference in char gasification kinetics for Hargassner simulations

Kinetics for secondary Tar cracking reactions	
Sim	Kinetics
Hargassner 1	Liden
Hargassner 2	Liden
Hargassner 3	Rath
Hargassner 4	Morf
Hargassner reci.	Liden

Table 22: Kinetics for sec. tar cracking for Hargassner sim.

The gasification reaction kinetics are adopted from the Gas 1 simulation. Furthermore, the water gas shift of Biba was added to the simulation. The gas phase reactions were adopted from the Daouk simulations, and the tar cracking rate from Daouk 2. For the pyrolysis scheme, oxidative pyrolysis was used. The input for fuel and the gasification medium is similar to the ones of the Daouk simulations, where the oxidative pyrolysis scheme is used as well. Additionally, to the validated reactions listed above, secondary tar cracking reactions were added. A detailed list of all the kinetics used for each simulation can be seen in Table 25.

For secondary tar cracking, three sets of kinetics are presented in this master thesis. The fastest kinetics (Liden) managed to almost reduced the tars to zero. The kinetics for each simulation are shown in Table 22. The mass yields of secondary tar can be seen in Figure 28. For the secondary tar cracking, steam reforming is considered, as benzene is a more refractory compound but steam

can accelerate the cracking process. The yields for the secondary tar cracking products shown in Table 23.

Secondary tar cracking	
Yields	
CO [-]	2.153846154
H_2O [-]	-1.384615385
CO_2 [-]	-
H_2 [-]	0.230769231
O_2 [-]	-
CH_4 [-]	-
C_2H_4 [-]	-
C_6H_6 [-]	-1
Tar [-]	-
N_2 [-]	-
Reaction enthalpy [kJ/kg]	9498.9

Table 23: Secondary tar cracking yields

To stabilize the simulation and get a more even heat distribution throughout the reactor, the fire stone of the gasifier was modelled with a constant temperature of 1050K at 0.01 m under the surface, which was based on measured data.

Firestone assumptions		
λ [W/(m*K)]	L [m]	T [K]
1.5	0.01	1050

Table 24: Firestone assumptions

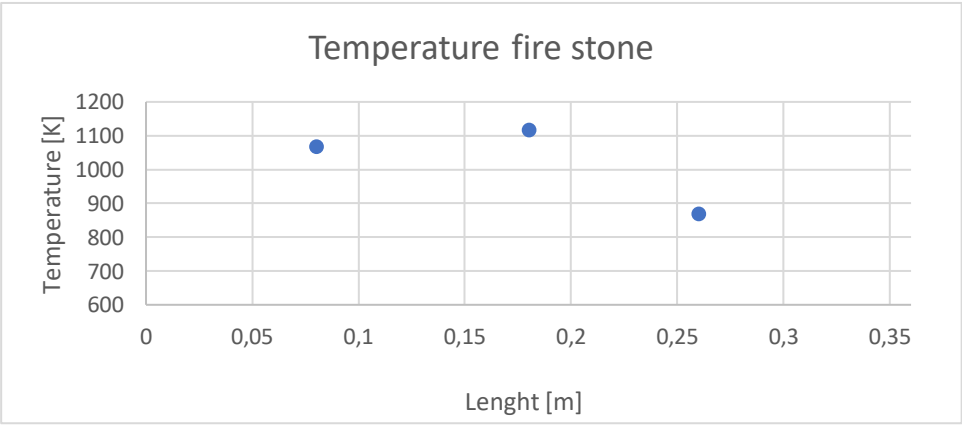

Figure 23: Measured temperature of firestone

Sim	Harg.1	Harg. 2	Harg. 3	Harg. 4	Harg. recirc.
Mass in Gas [kg/h]	32.8	32.8	32.8	32.8	35.54
Mass in Solid [kg/h]	18.49	18.49	18.49	18.49	16.06
MOIST_IN	0.1	0.1	0.1	0.1	0.1
NGRID_REACTOR	40 [1;1;1;1;1;1]	40 [1;1;1;1;1;1]	40 [1;1;1;1;1;1]	40 [1;1;1;1;1;1]	40 [1;1;1;1;1;1]
NRXN	14	14	14	14	14
tstop	100	100	100	100	1
tsave	2	2	2	2	100
deltat	1	1	1	1	2
POROSITY_REACTOR	0.6	0.6	0.6	0.6	0.6
R_PART_0	0.005	0.005	0.005	0.005	0.005
R_REACTOR	0.08	0.08	0.08	0.08	0.08
L_REACTOR	0.36	0.36	0.36	0.36	0.36
Pyrolysis	Oxidative	Oxidative	Oxidative	Oxidative	Oxidative
Mass _In	Biomass	Biomass	Biomass	Biomass	Biomass
Y_GAS_IN	Air	Air	Air	Air	CO2: 5.74% O2: 18.49% N2: 75.77%
F_GAS	1	2	2	2	2
LAMBDA_INS	1.5	1.5	1.5	1.5	1.5
L_INS	0.015	0.015	0.015	0.015	0.015
E_LOSS_TOP	0	0	0	0	0
E_LOSS_DOWN	10000	10000	10000	10000	10000
THERM_CONDUC_WOOD	0.2	0.2	0.2	0.2	0.2
Temperature fire stone	1050	1050	1050	1050	1050
T_IN_G[K]	300	300	300	300	300
T_IN_SOLID[K]	300	300	300	300	300
Water gas shift	Biba	Biba	Biba	Biba	Biba
Gas phase oxi. reaction					
CO	Jensen	Jensen	Jensen	Jensen	Jensen
H2	Gomez Barea I	Gomez Barea I	Gomez Barea I	Gomez Barea I	Gomez Barea I
CH4	Jones-Lindstest	Jones-Lindstest	Jones-Lindstest	Jones-Lindstest	Jones-Lindstest
Tar Cracking					
Primary	Liden	Liden	Liden	Liden	Liden
Secondary	Liden	Liden	Rath	Morf	Liden

Table 25: Relevant data for Hargassner simulations

5.1 Evaluation of the results Hargassner simulations

The diagrams for the simulations, represent the Hargassner 2 simulation. Biomass and the gasification medium enter the reactor at 0.36m and the producer gas exits at 0m. Such as with the diagrams depicted in chapter x, the flow direction is indicated by an arrow. The diagrams and results for the recirculation simulation are shown later in chapter

5.1.1 Diagrams for Hargassner 2 Gasification

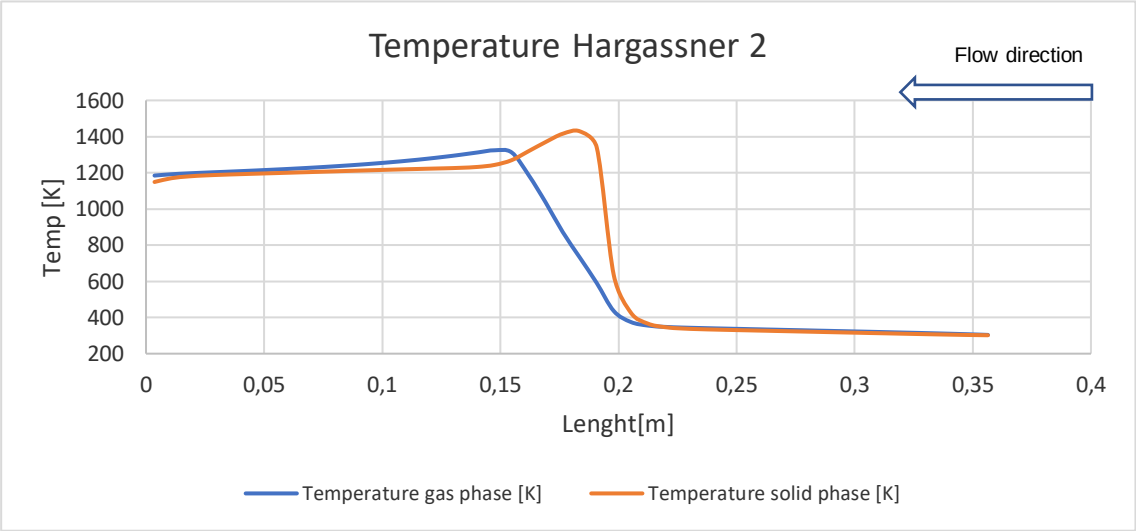

Figure 24: Temperature Hargassner 2 simulation

Figure 25 shows the mol yields for the simulation. The pyrolysis starts at 0.2 m, then the oxidation reaction sets in, which is expressed as dents in the CO, H_2 and CH_4 curves. After the oxygen is used, the gradient of these curves increases and H_2 and CO are produced through gasification. Because of the fast tar cracking reactions, the tars are nearly decreased to zero.

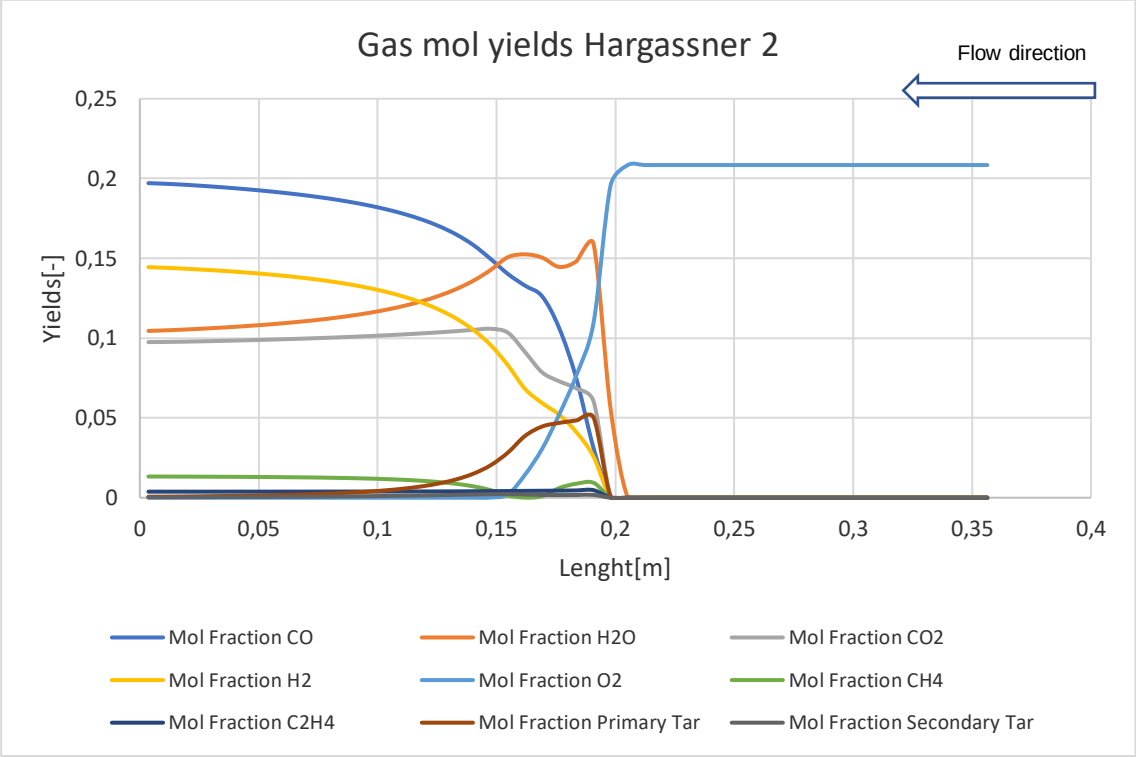

Figure 25: Mol yields Harg. 2 simulation

Figure 26 shows that the pyrolysis is incredibly fast, and all biomass is converted, starting at 0.2 m. The charcoal mass decreases then through oxidation and later, at a much slower rate, through gasification.

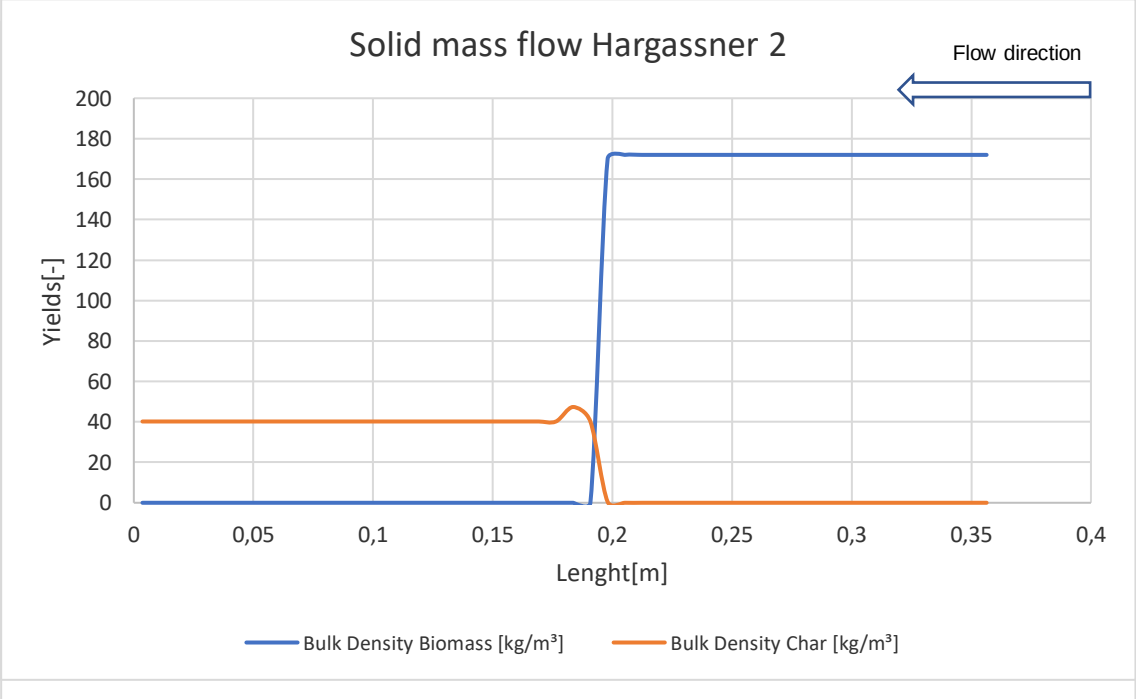

Figure 26: Solid mass flow Harg. 2 simulation

Figure 27 shows the comparison between the temperatures of the experiment and the simulation. As mentioned previously, the temperature curves can be used to locate the oxidation front. The difference between the oxidation front of the experiment and the simulation is within a tolerable range. The heat releases for the simulation are shown in Table 26.

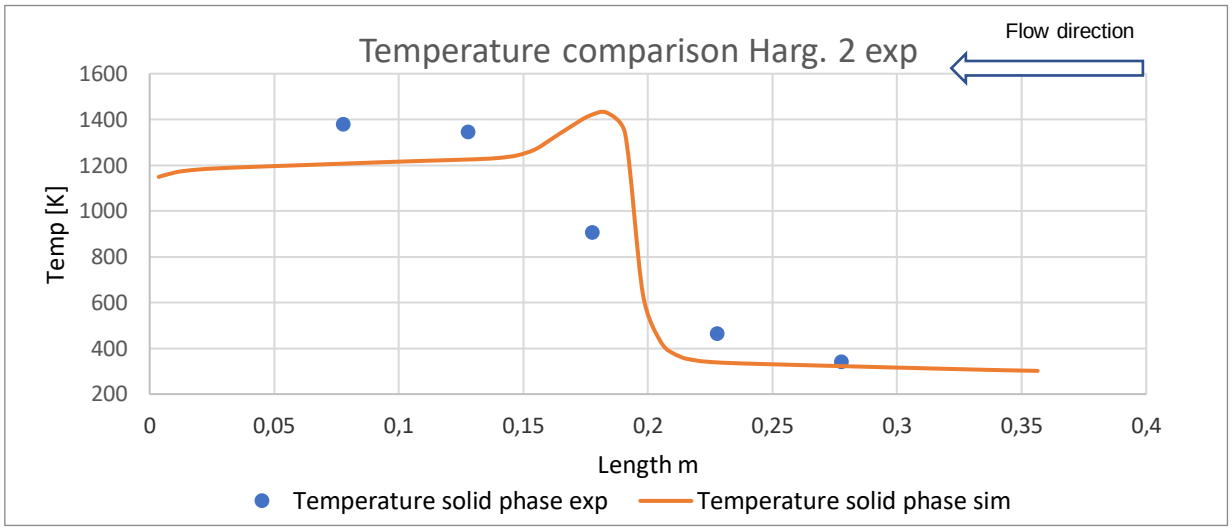

Figure 27: Temperature comparison experiment Harg. 2 simulation

Table 26 shows the heat realises for the Hargassner simulation. The negative lateral heat release is due to an assumed constant temperature of 1050K for the firestone.

Heat release Hargassner	
Heat release top [kW]	0.0000
Heat release bottom [kW]	0.2011
Lateral heat release [kW]	-0.7925
λ [W/(mK)]	1.5
L [m]	0.015

Table 26: Heat release Hargassner

Figure 28 shows the difference of the mass yields for different secondary tar crack reactions kinetics. The Liden kinetics, which are the fasters, reduce the amount of tars significantly. The slowest reaction kinetics (Rath) show not much of a reduction at all.

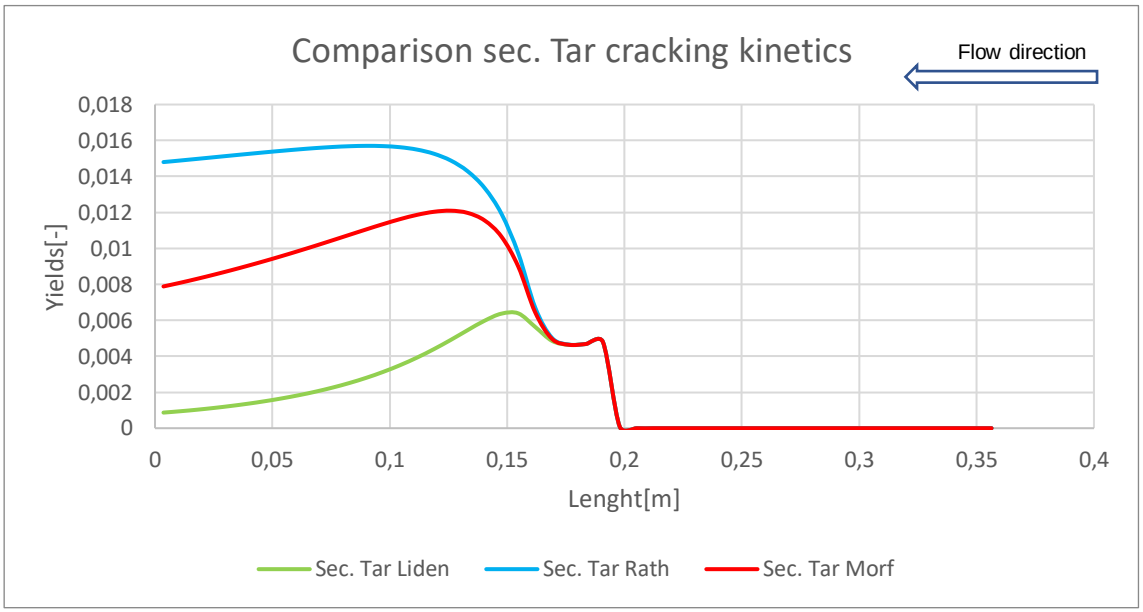

Figure 28: Comparison sec. tar cracking between Harg.2 (Liden) Harg.3 (Rath) Harg.4 (Morph)

5.1.2 Diagrams for Hargassner recirculation

Figure 29 depicts the temperature for the recirculation simulation. The values are a bit lower than for the previous simulations due to of the lower oxygen amount in the gasification agent.

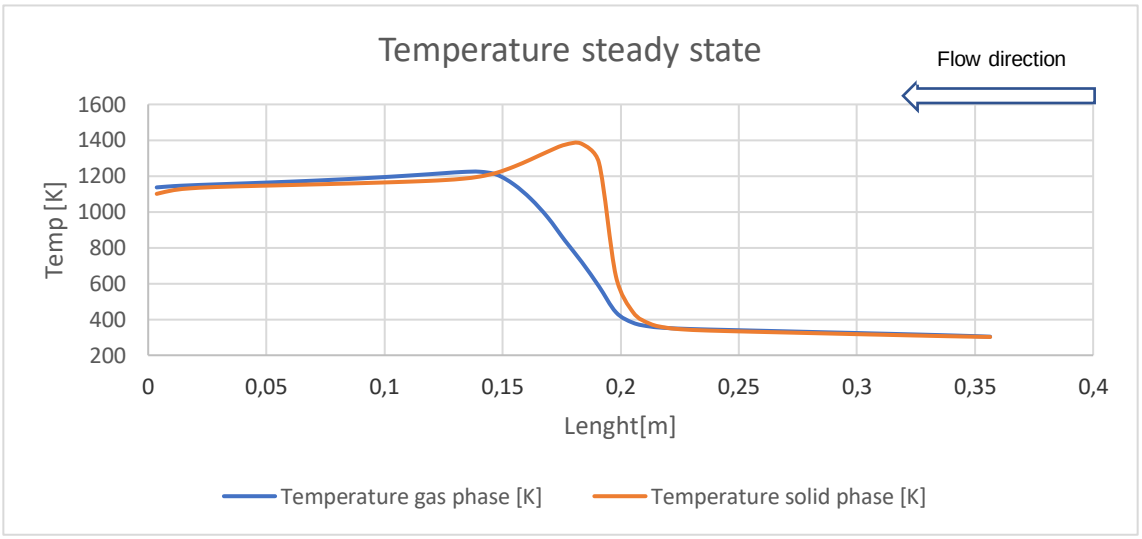

Figure 29: Temperature recirculation

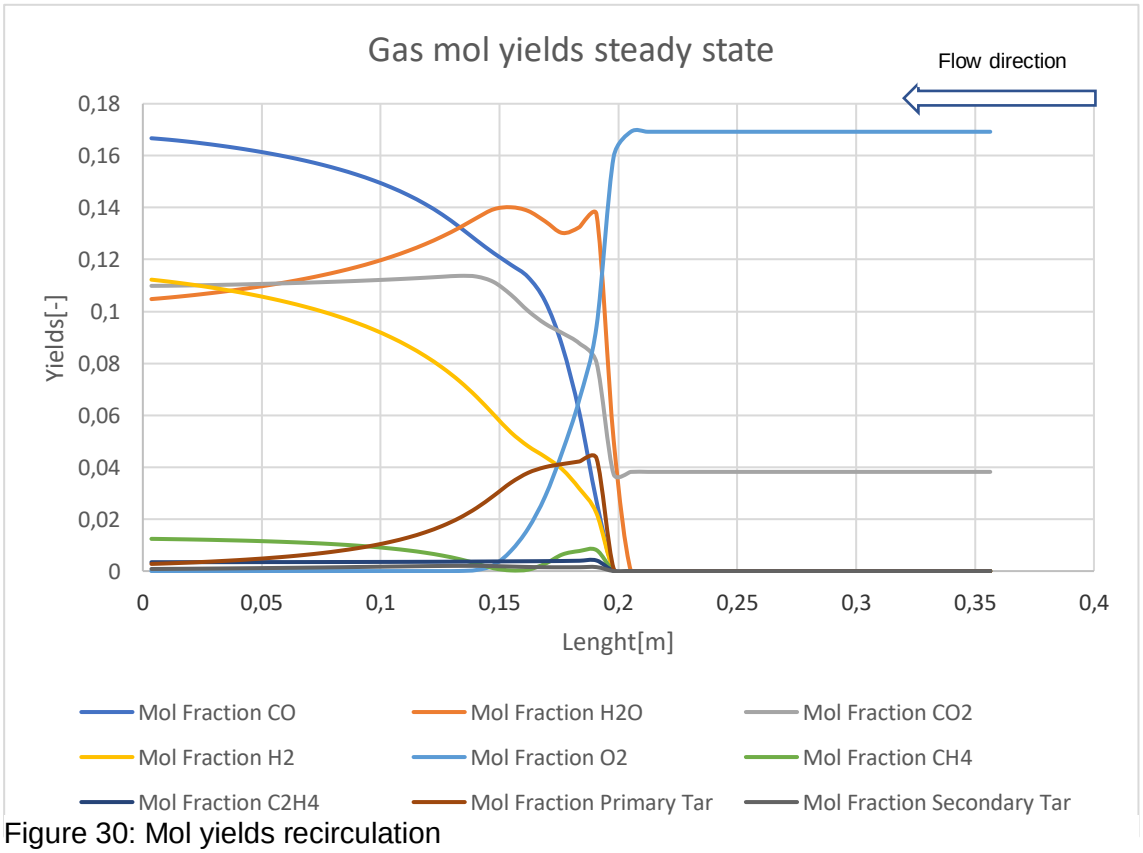

Figure 30: Mol yields recirculation

5.1.3 Discussion of the Hargassner results

For the Hargassner simulation, the oxidative pyrolysis was necessary to get more stable results as well. The reason for the necessity of the oxidative pyrolysis was already discussed in the Daouk simulations. Without the oxidative pyrolysis, there was too much oxygen left in later stages. That had led to problems in the oxidation zone, were the mass flow for the charcoal was reduced to zero. Due to their higher air-fuel ratio, this issue is more relevant for the Hargassner simulations.

For the gas phase oxidation reactions, the same set of kinetics as for the Dauok 1 simulation were used. The water gas shift reactions are activated in this simulation and helped getting a more accurate yield composition compared to the producer gas.

The difference between the Hargassner 1 and Hargassner 2 simulations are the reaction kinetics for the gasification of charcoal. Hargassner 2 has faster reaction rates and, therefore, a higher proportion of CO and H_2 in the yield composition. Also, more charcoal is converted in Hargassner 2 , due to the faster kinetics.

For both simulations, the temperature of the firestone was set to 1050K. That constant temperature helped to stabilize the process and improved the gasification behaviour, which led to a larger amount of CO and H_2 in the simulations. It further helped to get a more accurate yield composition compared to the experiments. (Table 28)

The simulations for the Hargassner recirculation predicted the reduction of the temperature, due to the lower amount of oxygen. It also showed the change in the producer gas combustion. The shift of the oxidation front which was measured in the experiment, did not occur in the simulation. The position of the oxidation front is very rigid in the simulations. The results for the recirculation simulation are shown in Table 29.

Harg. 2, 3, and 4 all use the same kinetics for char gasification. The difference between these simulations is the reaction rate for the secondary tar cracking. Harg. 2 has the faster kinetics and, therefore, the lowest amount of secondary tar. The difference between the tar cracking kinetics can also be seen in Figure 28.

For the comparison of the tar content between the simulations and the experiments a tar protocol was only available for the gravimetric tars, which are the heavy fractions of the tars. The real amount of tars is therefore higher than the amount of gravimetric tars. Also because of the high deviation between experiments with the same parameters the average of 4 tar protocols was taken. Table 27 shows a comparison between the gravimetric tars of the simulations. The experimental amount of the gravimetric tar was very low so the fastest tar cracking kinetics (Liden) were selected, which were used in the Harg. 1 and Harg. 2 simulations.

The simulation Harg. 2 has best fitting parameters to describe the gasifier. The following processes are now accurately described by the simulation: oxidative pyrolysis, water gas shift, oxidation reactions, char gasification and tar cracking.

Comparison tar content					
Sim	Harg.1	Harg. 2	Harg. 3	Harg. 4	Experiment
Prim tar [kg/h]	0.02345	0.08052	0.03230	0.04651	-
Sec. tar [kg/h]	0.01594	0.04407	0.75828	0.40265	-
Sum tars [kg/h]	0.03939	0.12459	0.79058	0.44916	-
Gravimetric tar average[kg/h]	-	-	-	-	0.03783
Gravimetric tars average [mg/m^3]	-	-	-	-	210

Table 27: Comparison tar content between simulations and experiments

Mol yields [%]	Experiment	Harg. 1	Harg. 2	Harg.3	Harg.4
CO	19.85%	18.59%	19.71%	19.23%	19.55%
H2O		11.23%	10.25%	12.36%	11.32%
CO2	8.75%	10.20%	9.80%	9.54%	9.62%
H2	15.06%	13.94%	14.71%	11.97%	13.29%
O2		0.00%	0.00%	0.00%	0.00%
CH4	1.68%	1.31%	1.34%	1.36%	1.34%
C2H4		0.38%	0.38%	0.39%	0.38%
Prim. tar		0.03%	0.06%	0.03%	0.04%
Sec. Tar		0.01%	0.03%	0.48%	0.25%
N2		44.31%	43.78%	44.62%	44.18%
Unconverted mass		5.97%	4.10%	1.85%	2.85%
H2O yields wt[%]	10.75%	8.21%	7.51%	8.80%	8.17%
Mass error		0.04%	0.02%	0.02%	-0.02%
Enthapy error		-2.78%	-2.83%	-3.00%	-2.94%

Table 28: Mol yields producer gas Hargassner

Mol yields [%]	Experiment [kg/h]	Sim[kg/h]	Mol yields [%]
CO	10.77	9.26	16.67%
H2O		3.74	10.48%
CO2	7.74	9.59	10.98%
H2	0.48	0.45	11.22%
O2		0	-8.43E-09
CH4	0.5	0.39	1.24%
C2H4		0.19	0.34%
Prim. tar		0.34	0.27%
Sec. Tar		0.12	0.08%
N2		27.05	48.71%
Mass error			-0.02%
Enthalpy error			-3.05%

Table 29: Comparison between experiment and simulation for Hargassner recirculation

5.1.4 Atom balances Hargassner simulations

The balances for mass enthalpy and the atom balances are all closed. The minor error for enthalpy balances has the same reasons like mentioned in the previous chapter.

To evaluate the simulation, the atom balances are shown in Table 30 and Table 31.

Atom balances Hargassner 2				
	C	H	O	N
Input Mass %	16.5403609	2.35234056	31.9520608	49.1552378
Output Mass %	16.5418038	2.3262727	31.9652438	49.1666797
Difference	-0.00144297	0.02606786	-0.013183	-0.01144189

Table 30: Atom balances Hargassner

Atom balances Hargassner recirculation				
	C	H	O	N
Input Mass %	15.3592483	2.03091534	30.4205701	52.1892662
Output Mass %	15.360453	2.00864555	30.4313442	52.1995573
Difference	-0.00120468	0.02226979	-0.01077403	-0.01029109

Table 31: Atom balances Hargassner recirculation

5.2 Tips for running the simulation

In course of this master thesis, know-how of how to run the simulation code was created. The following tips should help for future simulations.

5.2.1 Pointers for starting a new simulation

When starting a new simulation, the following reactions and functions were deactivated: water gas shift, oxidative gas phase reaction, tar cracking and lateral heat loss. This makes the code faster for the first attempts and helps to identify possible causes of system or code failure.
If the gasification medium contains oxygen, the first-time steps tend to have a negative dry solid unconverted mass, which becomes positive after some time steps.

5.2.2 Preventing negative dry unconverted mass

There are two main methods to prevent the dry solid negative mass to become negative, lowering the temperature, or lowering the oxygen yield in the control volumes where charcoal is present. For this method it is recommended to use a previous solution as a starting point. If the dry solid unconverted mass stays negative, it is not possible to activate the lateral heat loss. The following methods can help:
Activation of the oxidative gas phase reactions helps to consume the oxygen, therefor there is none, or less oxygen left for charcoal gasification. If this is not enough it is also possible to apply a heat loss from the bottom.
If this does not prevent the negative unconverted mass the next step is to reduce the mass flow of the inlet gas to the point were no negative unconverted mass occurs. When the system is ready, then it is possible to activate the lateral heat loss. With the steady solution of this simulation the next simulation can be started with the needed amount of inlet gas mass flow. If it is not possible to achieve a positive dry solid unconverted mass, the gas mass can be set at the amount where no negative mass occurs. Then, tar cracking can be activated. Secondary tar cracking is endothermic and, therefore, decreases the temperature.
If the solution is then steady and no negative dry solid unconverted mass occurs, the previous deactivated functions can be activated.

5.2.3 General pointers

If the simulation is running stable, it is recommended to use the stable solution as the starting point for new simulations.
When the quantity of a parameter is changed by a large factor, the simulation could crash. To prevent this from happening, the parameter can be altered in smaller steps up to the desired magnitude. The solution of the previous step is then used to calculate the next one, until the last solution is calculated.
Are the control volumes too tight, the simulation crashes occasionally as the code is unable to set the step size to the required very small time step

6 CONCLUSIONS

The aim of this master thesis was to understand the downdraft gasification in more detail, due to its limitations and difficult to control oxidation zone. To analyse this process, a 1-dimensional flow model was developed. To validate the model, experimental data was used from either literature, or data generated by the gasifier at the institute.

Because of the complex nature of the simulation of downdraft gasification, the evaluation strategy was to divide the model into smaller sub-processes, to find literature, where these sub-processes are well described, and to compare the results of the simulation with the experimental data. The sets of data, which had been compared, include the mol yield composition of the producer gas, the temperatures in the reactor, and the position of the oxidation front. To further evaluate the simulation, the bulk density and the mass flow of the solid species were plotted for each simulation. Also, the enthalpy error was considered in the evaluation as well as the difference between the input and output mass. Furthermore, the atom balances were considered for each of the simulations, where the in- and output of carbon, oxygen, nitrogen, and hydrogen were compared. All considered atom balances were well closed.

The first sub-process, which was validated, was the char gasification zone. The reaction kinetics used for the first sets of simulation were the same ones used by the previous model for updraft gasification. After comparing the yield composition of the in- and output, the kinetics were modified and multiplied with a factor. To further improve the yield composition of the producer, gas water gas shift was added. The kinetics that have been selected after this step are shown Table 7.

After the reaction kinetics for the char gasification zone had been set, the pyrolysis and the oxidation zone were investigated. For the validation, experimental data from literature was used, where biomass is gasified at a low air-fuel ratio ($\lambda = 0.11$). Both zones are crucial for the stability of the system. For the first simulation, an inert pyrolysis was used, which had led to unstable conditions. To stabilize the simulations, an oxidative pyrolysis scheme was introduced (see Table 15), which is based on the inert pyrolysis scheme. The reaction kinetics for the char oxidation were taken from the updraft gasification and proved to be fitting. For the gas phase, oxidation reactions of CO CH_4 and H_2, several reaction kinetics from literature were tried out. The results of the producer gas composition were than compared with the experimental results. The set of reaction kinetics that produced results closest to the experimental results were then taken (see Table 7). Because the oxidation zone is essential for the stability of the entire system, the reaction set of reaction rate was checked for stability by analysing the mass error. A steady state of the simulations is achieved when the mass error is below 0.1%. It is highly important to keep the tar content in the producer gas minimal with downdraft gasification for CHP. In this stage of the simulation, reactions for primary tar cracking were added. Like in previous stages of the simulation, tar cracking rates were adopted from literature and implemented in the simulation. The comparison between three different reaction rates can be seen in Figure 20 and Table 27.

After, the reaction kinetics and product schemes were validated for the sub-processes. The acquired know-how was used to choose the reaction kinetics for the simulation of the entire process. The kinetics and reactions which were used are shown in Table 25.To improve the accuracy of the simulations, secondary tar cracking reactions were added. To stabilize the process further and to increase the amount of gasification, a constant temperature was set for the

firestone, which is based on experimental measurements. These temperatures should mimic the distribution of heat due to conduction in the firestone, which occurs in the real application. This modulation also helped to increase the charcoal gasification amount, which improved the results compared to the experiments. As in the previous steps, the results were then validated by comparing them with the experimental data. Furthermore, the mass error enthalpy error, and atom balances were checked.

The validation of the model showed that (when the right kinetics were selected) the representation of the producer gas yields is fairly accurate (the error is in a range of 2% absolute at the maximum). The position of the oxidation front was well predicted for the simulations Harg. 1 – 4 and also for the Daouk simulations. For the recirculation simulations the change of the position for the oxidation front was not depict by the simulation, due to it seems that the position of the oxidation front is very rigid for the simulations.

The pyrolysis occurs fast and the front is very thin. The simulations are much more stable with the oxidative pyrolysis scheme and with higher air-fuel ratio, however, that is only possible when the oxidative pyrolysis is used. Because of its exothermic nature, the oxidative pyrolysis helps to provide extra heat for the heating and drying zone at the top of the reactor. This helps to keep the process autothermal. Especially for simulations with a higher air-fuel ratio, like the Hargassner simulations, the oxidative pyrolysis keeps the amount of oxygen lower for the oxidation zone, which further stabilizes the process.

The gas phase oxidation reactions manly influence the yield composition but can also lead to unstable conditions when unfitting reaction kinetics were chosen. The tar cracking reactions had no influence for the stability of the system for the simulations which were executed. They only influenced the yield composition.

The suitable kinetics and product compositions, for fixed bed downdraft gasification, were found for char gasification, water gas shift, oxidative pyrolysis, gas phase oxidations, primary tar cracking and secondary tar cracking.

The model is now validated for downdraft gasification and can be used for future simulations. Because the simulations were done with a one-dimensional flow model, there are certain limitations. For further and more detailed investigations, a CFD model can be used for the future.

LITERATURE

[1] Kaltschmitt, M., & Hartmann, H. (2007). Energie aus Biomasse. Vorlesung, Institut für Umwelttechnik und Energiewirtschaft, Technische Universität Hamburg-Harburg, WS, 2008.

[2] Anca-Couce, et al. (2021). Bioenergy technologies, uses, market and future trends with Austria as a case study. *Renewable and Sustainable Energy Reviews*, *135*, 110237.

[3] Teixeira et al. (2012). Gasification of char from wood pellets and from wood chips: Textural properties and thermochemical conversion along a continuous fixed bed. *Fuel*, *102*, 514-524.

[4] Anca-Couce, A., & Obernberger, I. (2016). Application of a detailed biomass pyrolysis kinetic scheme to hardwood and softwood torrefaction. Fuel, 167, 158-167

[5] Mandl, C., Obernberger, I., & Biedermann, F. (2010). Modelling of an updraft fixed-bed gasifier operated with softwood pellets. Fuel, 89(12), 3795-3806.

[6] Grønli, M. G. (1996). A theoretical and experimental study of the thermal degradation of biomass. PhD thesis. Norwegian University of Science and Technology (NTNU).

[7] Di Blasi, C. (2004). Modeling wood gasification in a countercurrent fixed-bed reactor. *AIChE Journal*, *50*(9), 2306-2319.

[8] Biba, V., Macak, J., Klose, E., Malecha, J. (1978). Mathematical-model for gasi fication of coal under pressure. Industrial & Engineering Chemistry Process Design and Development, 17 (1), 92-98

[9] Daouk, E., et al. (2017). Oxidative pyrolysis of wood chips and of wood pellets in a downdraft continuous fixed bed reactor. *Fuel*, *196*, 408-418.

[10] Baumlin S, Broust F, Ferrer M, Meunier N, Marty E, Le´de´J. The continuous selfstirred tank reactor: measurement of the cracking kinetics of biomasspyrolysis vapours. Chem Eng Sci 2005;60:41–55.

[11] Hobbs et al. (1992). Modeling fixed-bed coal gasifiers. *AIChE Journal*, *38*(5), 681-702.

[12] Cooper, J., & Hallett, W. L. H. (2000). A numerical model for packed-bed combustion of char particles. *Chemical Engineering Science*, *55*(20), 4451-4460.

[13] Jakobsen, H. A. et al. (2002). A numerical study of the interactions between viscous flow, transport and kinetics in fixed bed reactors. Computers & chemical engineering, 26(3), 333-357.

[14] Gómez-Barea, A., & Leckner, B. (2010). Modeling of biomass gasification in fluidized bed. Progress in Energy and Combustion Science, 36(4), 444-509.

[15] Tsotsas, E. (2010). Heat and Mass Transfer in Packed Beds with Fluid Flow. In: VDI Heat Atlas. Second Edition (section M7), Springer-Verlag.

[16] Tsotsas, E. (2010). Thermal Conductivity of Packed Beds. In: VDI Heat Atlas. Second Edition (section D6.3), Springer-Verlag.

[17] Anca-Couce, A., et al. (2017). Online experiments and modelling with a detailed reaction scheme of single particle biomass pyrolysis. Journal of analytical and applied pyrolysis, 127, 411-425.

[18] Anca-Couce, A., & Scharler, R. (2017). Modelling heat of reaction in biomass pyrolysis with detailed reaction schemes. Fuel, 206, 572-579.

[19] Modelling fuel flexibility in fixed-bed biomass conversion with a low primary air ratio in an updraft configuration. A. Anca-Couce, G. Archan, M. Buchmayr, M. Essl, C. Hochenauer, R. Scharler. In review.

[20] Lettner F, et al. Biomass gasification - state of the art description. Gasification guide project. Deliverable 8. Intelligent Energy - Europe (IEE); 2007.

[21] Knoef HAM. Handbook of biomass gasification. BTG biomass technology group; 2015.

[22] Patra, et al. (2016). A comprehensive dynamic model for downdraft gasifier using heat and mass transport coupled with reaction kinetics. *Energy*, *116*, 1230-1242.

[23] Tinaut, et al. (2008). Effect of biomass particle size and air superficial velocity on the gasification process in a downdraft fixed bed gasifier. An experimental and modelling study. *Fuel processing technology*, *89*(11), 1076-1089.

[24] Simone, et al. (2013). Numerical and experimental investigation of downdraft gasification of woody residues. *Bioresource technology*, *133*, 92-101.

[25] Zachl, A. et al.(2021). Flame ionization detection as a simple real-time tar monitoring device for biomass downdraft gasification. *Fuel*, *289*, 119950.

[26] Winter R, Bach H. Biokraftstoffe im Verkehrssektor 2018. Bundesministeriums für Nachhaltigkeit und Tourismus Austria; 2018 (in German).

[27] Hein D, Karl J. Conversion of biomass to heat and electricity. Energy Technol: Renew Energy Landolt-Boerstein New Ser 2006;VIII/3C:374–413.

[28] Mitani, T., & Williams, F. A. (1980). Studies of cellular flames in hydrogen oxygen nitrogen mixtures. *Combustion and flame*, *39*(2), 169-190.

[29] Jones, W. P., & Lindstedt, R. P. (1988). Global reaction schemes for hydrocarbon combustion. *Combustion and flame*, *73*(3), 233-249.

[30] Dryer, F. L., & Glassman, I. (1973, January). High-temperature oxidation of CO and CH4. In *Symposium (International) on combustion* (Vol. 14, No. 1, pp. 987-1003). Elsevier.

[31] Jensen, A et al. (1995). Formation and reduction of NOx in pressurized fluidized bed combustion of coal. *Fuel*, *74*(11), 1555-1569.

[32] Liden, A. et al. A kinetic model for the production of liquids from the flash pyrolysis of biomass. *Chemical engineering communications*, *65*(1), 207-221.

[33] Rath, J., & Staudinger, G. (2001). Cracking reactions of tar from pyrolysis of spruce wood. *Fuel*, *80*(10), 1379-1389.

[34] Anca-Couce, et al. (2012). Smouldering of pine wood: Kinetics and reaction heats. Combustion and Flame, 159(4), 1708-1719.

[35] Huang, Y, et. al. (2020). Fundamental advances in biomass autothermal/oxidative pyrolysis: a review. ACS Sustainable Chemistry & Engineering, 8(32), 11888-11905.

[36] Salo K. Carbona gasification technologies. Biomass gasification plant in skive. In: Gasification 2010, Swedish gas centre (SGC); 2010 [Gothenburg, Sweden]

[37] Morf, P. O. (2001). *Secondary reactions of tar during thermochemical biomass conversion* (Doctoral dissertation, ETH Zurich).

[38] Anca-Couce et al. (2021) Modelling fuel flexibility in fixed-bed biomass conversion with a low primary air ratio in an updraft configuration, Fuel, 296, 0016-2361.